

GeoArch

Report 2025/01

Ironworking residues from Llanfairfechan
(G2495)

Dr Tim Young
13th March 2025

Ironworking residues from Llanfairfechan

Dr T.P. Young

Abstract

The assemblage from the project comprised a total of approximately 100 significant pieces, plus some fine debris (total 1.7kg). The majority of this material (1.6kg) derives from a deposit of smithing waste, believed to be of 12th- 13th century age) investigated in adjoining test pits 16 and 73 at Ty'n y Llwyfan. This smithing waste formed the focus of the analytical investigation.

The waste was investigated through bulk analysis of one sample of smithing hearth cake (SHC) and one piece of hearth ceramic and through microanalysis of microresidues. The SHCs are suggestive of light or intermittent work, although the assemblage was too small to make definite interpretation. The microresidues suggest high temperature forging, including welding employing the use of a quartz flux. The analysis suggested that the iron being worked was dominantly phosphoric and perhaps ultimately from a bog iron source. Flake hammerscale (FHS) was present as particularly large and shiny fragments, possibly because of their separation from the iron substrate through the development of a phosphorus-rich detachment zone. The use of the welding flux appears sparing, perhaps because the iron welded easily.

The purpose of the smithing is unknown, but included forging and welding, so was more than just light farrier work for instance, but equally it does not appear to have been intensive.

Contents

Abstract	1
Contents	1
Methods	1
Project rationale and history	1
Analytical methods	1
Results	2
General	2
Iron-working (blacksmithing) residues	2
Description of the ironworking macroresidues	3
Description of the ironworking microresidues	3
Details: samples examined by ASEM	3
Sample LFF1	3
Sample LFF2	4
Interpretation	4
Discussion	5
Figure captions	7
References	8
Table 1: summary catalogue	9
Table 2: major element analyses by XRF	11
Table 3: trace element analyses by ICP-MS 1 ...	11
Table 4: trace element analyses by ICP-MS 2 ...	11
Table 5: estimated composition SHS	12
Table 6: properties of SHS	13
Table 7: estimated composition FHS.....	14
Table 8: properties of FHS.....	15
Table 9: analyses of FHS inner slag.....	16
Figures	17
Appendix A: archive of DS data	
Appendix B: archive of BSEM images	

Methods

Project rationale and history

This assessment was conducted in August 2024 and was commissioned by Jane Kenney of Heneb. The materials derive from a programme of test-pitting undertaken by the former Gwynedd Archaeological Trust as part of the *Landscape of Neolithic Axes Project* (Project G2495).

The assessment resulted in the statement (Young 2024, 2):

'The evidence for the smithing is slightly unusual, particularly in the nature of the hammerscale present. A limited analytical investigation of the scale and the associated macroresidues is recommended to enable further clarification of the purpose of the activity.'

The analysis phase of the work was designed around two components: firstly the bulk elemental analysis of an example of a smithing hearth cake from the assemblage (a 125g example from <1605>, context (1603)) and of a fragment of hearth cermaic (from <7309>/<7312> from context (7305), secondly analytical electron microscopy of micro-residues via separate strew mounts of tabular and spheroidal particles (flake and spheroidal hammerscale).

Analytical methods

Bulk chemical analysis was undertaken using two techniques. The major and minor elements (Si, Al, Fe, Mn, Mg, Ca, Na, K, Ti, P and S) were determined on a fused bead using wavelength-dispersive X-Ray fluorescence (WD-XRF). Whole-specimen chemical analysis for thirty-six trace elements (Be, Sc, V, Cr, Co, Ni, Cu, Zn, Ga, Rb, Sr, Y, Zr, Nb, Mo, Sn, Cs, Ba, La, Ce, Pr, Nd, Sm, Eu, Gd, Tb, Dy, Ho, Er, Tm, Yb, Lu,

Hf, Ta, Th, and U) were undertaken using a sample in solution by Inductively-coupled Plasma Mass Spectrometry (ICP-MS). Both XRF and ICP-MS analyses were commissioned from ChemoStrat Ltd (Welshpool, UK).

For XRF analysis, samples were ground using a tungsten carbide shatter mill, dried at 105C overnight and then 0.5g was mixed with 6.5g of 50:50 LiT/LiM flux and fused to produce a glass disk using a Claiss M4 Fluxy automatic fused disk maker. The samples were analysed using a Bruker S4 WDXRF using the default wavelengths for the elements identified. Calibration was via a selection of iron slag reference materials and geological reference materials.

Samples for trace elemental analysis by ICP-MS were drawn from a second aliquot of the powdered material using the alkali fusion method (Jarvis & Jarvis 1992a and 1992b; Pearce *et al.* 1999). Once prepared, the samples were then all subjected to analysis using a Thermo Scientific XSERIES 2 ICP-MS. Data quality was strictly monitored in terms of precision and accuracy by five international rock standards of known concentration and varying compositions which are run after every 20 unknown samples. In addition, external monitoring of data quality is carried out four times a year via the GeoPt round robin proficiency testing program (<http://www.geoanalyst.org/overview.html>).

The results of the elemental analyses are presented in Tables 2, 3 and 4 of this report.

Polished blocks for investigation on the SEM were prepared in the School of Earth and Ocean Sciences, Cardiff University. Electron microscopy was undertaken on the Zeiss Sigma HD Field Emission Gun Analytical Scanning Electron Microscope (aSEM) in the School of Earth and Ocean Sciences, Cardiff University. Images presented here include backscattered electron photomicrographs (BSEM) to illustrate microstructures and secondary electron images (SEI) for the recording of loci of microanalysis. Microanalysis was undertaken using the system's energy-dispersive x-ray analysis system (EDS) controlled by Aztec software. The Astimex olivine, pyrope and magnetite standards were employed calibration process. The assistance of Dr Duncan Muir is gratefully acknowledged.

The GeoArch site code used for the samples is LFF. The microanalytical data are presented in Appendix A. SEM images of all areas are included in Appendix B, including, where appropriate, details of the analysed points/areas on SEI images.

All EDS analyses were collected with all elements analysed (including oxygen, but not carbon; all samples were carbon-coated). Area analytical totals were frequently far from 100%, because the analytical system is designed to provide totals of 100% from spot analyses in the centre of the field. The area analyses required for this project are not standardised in the same way and will diverge from a total of 100% (either above or below, depending on the location of the area #with respect to the centre of the field). In order to make the microanalytical results simply comparable across materials (and also sites), no attempt has been made to adjust for the oxidation state of elements with variable valency. The figures employed in the report have therefore been constructed with elements expressed as oxides in weight% calculated stoichiometrically and normalised, except for mineral structure calculations, where the measured oxygen has been used.

Throughout this report standard mineral terminology is applied to both natural and anthropogenic materials – although artificial phases are no longer strictly considered to be minerals.

All dates quoted in this report (unless specifically attributed as quotes) have been recalibrated using OxCal 4.4 with the IntCal20 calibration curve, rounded out to 10 years, and quoted as 2s, unless specifically stated.

Results

General

The assemblage submitted for assessment comprised a total of approximately 100 significant pieces, plus some fine debris (total 1.7kg). The majority of this material (1.6kg) derives from a deposit of smithing waste investigated in adjoining TPs16 and 73 at Ty'n y Llwyfan. TPs 75 and 40 each produced a single fragment of hearth ceramic and TP129 a small quantity of pyrotechnological residue from a, probably non-metallurgical, hearth.

The summary catalogue is presented as Table 1.

Iron-working (blacksmithing) residues

Investigation of the residues from ironworking (blacksmithing) were focused on materials from adjacent TPs 16 and 73.

Two contrasting suites of residues were recovered from the charcoal-rich spread in TP16 and from the pit in TP73.

The spread in TP16 (context (1603)) produced a small, dense smithing hearth cake (SHC) weighing 128g, an apparently 'double' SHC, with an upper conventional small, dense SHC attached to an obliquely-descending cake, possibly an earlier, displaced SHC, but with the two sharing a finely-dimpled surface. There was also a small fragment probably derived from a similar SHC. The overlying context ((1602)) yielded two small scraps of smithing slag.

In contrast, the fill of pit [7307] (context (7305)) produced several fragments of technical ceramic (total 192g) including fragments of a blowhole through the ceramic, as well as 16 fragments of slag (total 352g) comprising fragments from dense sheets, lobate flows and lower density blebby slags. Overlying contexts (7303) and (7302) produced small quantities of similar residues.

Context (7305) also produced an assemblage of smithing fines, comprising flake hammerscale (FHS), slag spheroids and rounded blebs, many of maroon-surfaced FAS/lining slag, some fired clay, some probably oxidised iron debris in thin sheets and some rare blebby pieces of dense slag. This context also produced an example of a 'fiddle-key' horseshoe nail, a type usually dated to the 12th-13th centuries. Two radiocarbon dates were obtained on oak charcoal from (7305): SUERC-130048 (1101±23BP) and SUERC-130049 (858±23 BP), which calibrate to cal. AD 890-1000 and to cal. AD 1150-1260 respectively. A date between the mid-12th and mid-13th centuries therefore seems possible, taking account the artefact and scientific evidence.

TP75 produced a fired clay fragment (from context (7505) possibly from the margin of a ceramic tuyère.

Description of the ironworking macroresidues from TPs 16 & 73

The most significant elements of the macroscopic assemblage from TPs 16/73 were two smithing hearth cakes (SHCs), both from TP16 <1605> from (1603).

SHCs are slag cakes that form just below the air input, from a mixture of iron (or iron oxide) lost from the workpiece and melted hearth lining, with lesser contributions from the fuel ash and, where appropriate, from any welding flux employed by the smith. SHCs are typically approximately plano-convex in shape, with a rounded base and a sub-triangular to sub-oval shape in plan.

Firstly from (1603) there was a 'double' SHC with an overall weight of 166g. This comprised an upper component, measuring 50x90x20mm, possibly slightly deformed by folding, attached to lower component, measuring 35x60x15mm; inclined in such a way that the two are continuous on one side. The base is finely prilly with fuel impressions and rust; the top is smoothish, dimpled with only a faint hint of lobes. This example was not examined in further detail. 'Double' SHCs are formed when the smith displaces the accumulated slag downwards to clear space in front of the blowhole, rather than removing it from the hearth.

Secondly, a straightforward, single, dense SHC, weighing 128g and measuring 60x70x30mm. It is crudely plano-convex. The top has fine fuel impressions on a poorly lobate surface, partly obscured by rust. The base is also crudely lobate, but rusty, with abundant adhering flake hammerscale. The SHC is internally vesicular, with simple subspherical vesicles up to approximately 4mm with more complex larger ones, some still containing charcoal remnants, up to 10mm.

The elemental composition of this piece was determined on a full-thickness sample (LFF4). The analysis (Tables 2-4) shows a high iron content (68.6% when expressed as FeO), a moderately high silica and alumina (18.7% and 4.7% respectively; with $\text{SiO}_2/\text{Al}_2\text{O}_3 = 3.9$). The alkalis and alkali earth elements are present in very low concentrations, with manganese and phosphorus both also low (with 0.15% MnO and 0.27% P_2O_5). The upper crust normalised rare earth element (REE) profile (Figure 1) is relatively flat, with a very similar shape to that of the analysis of a ceramic sample (LFF3), but slightly relatively depressed in the light REE (LREE). SHCs from blacksmithing typically have the largest non-iron input from the hearth lining, which thus supplies most of the REE.

The assemblage from TPs 16 and 73 includes several other pieces of dense iron slags, including a possible incipient SHC, fragments from SHCs and fragments from flows from the hearth floor. There were also many fragments of fired clay, indicative of a placed clay pit lining or, more likely an upstanding hearth wall. Several pieces of hearth ceramic showed evidence for the margin of a blowhole but were insufficient to determine whether the blowhole was located within a simple clay wall or within a preformed ceramic tuyère.

Description of the ironworking microresidues from TPs 16 & 73

The fill of pit [7307] (context (7305)) produced a rich assemblage of microresidues.

The true microresidues include, dominantly, flake hammerscale (FHS; in this assemblage of unusually large size), with lesser quantities of spheroidal hammerscale (SHS). The coarser microresidues (passing up strictly into macroresidues) include slag spheroids, slag blisters and slag flats. Sub-sampling of the microresidues from <7311> (7305) was undertaken to provide separate strew mounts of SHS (LFF1) and FHS (LFF2)

Hammerscale is associated with the superficial oxidation of iron at high temperature (Young 2011b), with FHS mostly indicative of the solid (or semi-solid) oxide layer spalling from the workpiece, whereas SHS forms from the air chilling of spatter from the molten oxide layer (often melted under the influence of a smithing flux) expelled from the join during forge (or fire) welding.

Slag spheroids are droplets of smithing slag that cooled within the fuel bed of the hearth, without amalgamating into a large mass. Slag blisters are probably mostly formed as flake hammerscale, but are lifted off the surface of the underlying metal by build-ups of gas (in some cases above underlying inclusions in the iron). Slag flats are thin skins of slag that form either on the surface of the workpiece or a tool.

Details: samples examined by ASEM

Sample LFF1

The sample of SHS particles is shown in Figure 2.

31 particles were investigated (Tables 5 and 6). For each particle (except S20) a bulk analysis by EDS was attempted, with a focus on areas devoid of voids, because some larger voids were observed on the SEM to contain small quantities of polishing medium (alumina powder). In a proportion of cases, it was not possible to analyse areas without any visible porosity, particularly for the more wustite-rich particles which contained little interstitial material. Those analyses for which careful inspection showed minor porosity have been categorised as 'slightly suspect', those with slightly coarser porosity very likely to have formed a trap for the polishing medium were categorised as 'very suspect'. Where possible, an estimate of the bulk composition of grains was determined by averaging the area analyses excluding the 'suspect' values, but in some cases, only 'suspect' regions were available for analysis, so this is noted in the table of compositions (Table 5)

The SiO_2 content of the SHS particles varies from less than 0.5% up to almost 22% (Figure 3). For SiO_2 contents of up to approximately 10%, the particles are dominated by stubby, complex, wustite dendrites and rounded, blebby 'pseudo-dendrites'. At above 10% SiO_2 , the wustite tends to be in finer, more delicate dendrites and is followed by either a glass or olivine, depending upon the rapidity of cooling. Most particles show a very thin superficial crust, in which magnetite is the dominant phase. Some particles, from across the range of SiO_2 content show the development of magnetite dendrites across the width of the particle before wustite follows.

Some particles show inclusions of unmelted quartz flux. This was mainly very small (<100µm), but in a few cases larger grains were preserved (in one case of 400 µm).

Seven particles showed fragments of unmelted oxide scale, lifted away from the iron substrate by the melted component (a process known as washing).

Small metallic prills were rare in the SHS. An example in S17 produced an analysis of approximately 95.2% Fe, 0.6% Co, 0.2% Ni, 3.2%As and 0.3% Sb and one from S32 of approximately 95.8% Fe, 1.4%Co, 2.0% Ni and 0.5% As (all in atomic%).

Sample LFF2

The sample of tabular particles is shown in Figure 4.

13 particles were investigated (Tables 7 and 8). For each particle either a bulk analysis extending across the whole thickness or a series of subareas spanning the thickness was attempted by EDS.

As with the SHS, analyses for which careful inspection showed minor porosity have been categorised as 'slightly suspect', those with slightly coarser porosity very likely to have formed a trap for the polishing medium were categorised as 'very suspect' (Table 7). Also for the SHS, 'suspect' particles may have slightly elevated Al_2O_3 at the expense of all other elements.

The tabular particles showed six varieties of microstructure (Figure 5):

- 1 (T3, T6): a neat, regular scale, with the magnetite and wustite zones developed evenly and with relatively constant thickness. There is little or no basal slag.
- 2 (T2, T4, T11, T12): a fairly neat scale, with a tendency to develop magnetite on both faces, in the absence of basal slag. Iscorite forms prominent 'stitching' between wustite grains in the lower part of the thickness.
- 3 (T9, T13): a neat regular scale, similar to (1), but developed over a thick layer of wustite-dominated basal slag.
- 4 (T1, T5, T8): scale retaining a thin outer magnetite zone, but the wustite zone has fragmented into slabs lying within a slag containing abundant new-formed wustite.
- 5 (T7): scale apparently showing the chaotic disaggregation of wustite, probably a new-formed wustite.
- 6 (T10): scale showing a siliceous composition with a quench texture including fine wustite dendrites. This has a very thin external crust.

Examples of scale of microstructural groups 1 to 3 all contain less than 4% SiO_2 , whereas those of groups 4 and 5 all contain 4% - 7% SiO_2 . The single example of group 6 contains 19% SiO_2 .

The compositional and microstructural difference between T10 and the remainder of the collection, means that it is probably best regarded as not flake hammerscale, but as a slag flat.

Small metallic prills were very rare in the tabular particles, but several examples were investigated within the fully melted tabular particle T10. These gave analysis of approximately 98.8% Fe, 0.6% Co, 0.1% Ni, of 98.8% Fe, 0.6% Co, and of 98.2% Fe, 0.6%Co, 0.2%Ni and 0.4% As.

Interpretation

The SHCs in the assemblage are small, the isolated example weighs 128g and the example with two fused masses (suggestive of accumulation in two work periods) weighs 166g. The SHCs are dense and well-formed, typical of those formed in a hearth using a ceramic tuyère or a blowhole in a ceramic wall, rather than an iron tuyère.

The elemental analysis of the individual SHC (LFF4) suggests it is equivalent to approximately 25% ceramic (of the composition of sample LFF3), plus 50% iron, 1.5% fuel ash and 6% silica (presumably from the flux). If the iron and phosphorus represent bulk loss of iron, then the iron contained 0.3%P, but such an estimate is speculative. The iron content of the ceramic is suspiciously high and the chosen sample may itself have been contaminated by iron from the hearth, even if that was not apparent when the sample was chosen. If the FeO content of the ceramic had only been 7% than the added iron would contribute around 55% of the SHC.

The content of MnO in the scale is generally rather low (Figure 7c, Figure 8c). One single piece of FHS shows strongly elevated MnO (T11) and some particles of SHS show very slightly increased levels with respect to the others. The source for Mn in these samples is likely to be inclusions of Mn-rich iron smelting slag present in the iron being worked

Analysis of the microresidues demonstrates that phosphorus is abundant in some particles and is particularly abundant in the basal (inner) slags (Figure 7b, Figure 8b). The migration of phosphorus from the iron to the slag phase as the iron is oxidised during scale formation contributes to both slag formation and scale detachment. (Young 2018, 21)

The content of alkali and alkaline earth elements in the SHS shows a rapid increase in particles over approximately 15% SiO_2 . In Figures 7a and 8a, this is demonstrated using the sum of CaO and K_2O . The SHS population has been divided into particles which do not show this enrichment (SHS (1)) and those that do (SHS (2)).

The SHS (1) group includes particles S2, S3, S4, S5, S6, S7, S8, S9, S11, S12, S13, S14, S15, S16, S17, S24, S25, S27, S28 and S30.

The SHS (2) group includes particles S1, S10, S18, S19, S21, S22, S23, S26, S29, S31 and S32.

The composition of the microresidues provides some insight into the process of SHS formation. The role of a quartz flux is significant. Its presence can be demonstrated not only by the relict quartz grains observed in 22% of the SHS grains examined, but also in the trend of increasing SiO_2/Al_2O_3 with SiO_2 content (Figures 7d and 8d) in the SHS grains in group SHS (1), reaching a peak value of approximately 10, very much higher than the value of 2.6 for the bulk analysis of the hearth ceramic (LFF3), or even the value of 3.9 for the bulk analysis of the analysed SHC (LFF4).

For SHS (2) particles, further increase in SiO₂ content is marked by a fall in SiO₂/Al₂O₃ and by elevated (K₂O + CaO). The fall in SiO₂/Al₂O₃ can be interpreted as an increased influence of the hearth ceramic, but the values for (K₂O + CaO) do not lie on such a trend – and these elements must be indicating, in addition, substantial incorporation of fuel ash.

The presence of a significant number of SHC particles in a compositional range with greater than 90% FeO and with FeO/(SiO₂+FeO) of greater than 95%, and with the wustite in those particles appearing to be new-formed with very little, if any, inherited solid phase, indicates that oxide scale was being melted under conditions with very low amounts of flux. That, in turn, indicates very high temperature conditions, probably in excess of 1300C. Such temperatures would be necessary for the welding of iron with a low carbon content.

Examination of the analyses of the residues on the FeO-SiO₂-Al₂O₃ ternary diagram (Figure 6, fields after Schairer & Yagi 1952) shows some of these same trends, with an array of analyses of group SHS (1) trending towards the SiO₂ pole, but that analyses of group SHS (2) become offset from this trend with slightly more aluminous compositions trending towards that of the hearth ceramic.

In summary, the microresidue assemblage suggests that much of the SHS (SHS (1)) was formed on the surface of phosphoric iron, enhanced by the use of a quartz smithing flux. The FHS (except particle T10) shows a similar influence, but an enhanced input from the fuel ash. A smaller proportion of the SHS (SHS (2) and particle (T10) formed under the additional influence of the hearth lining (as well as fuel ash). The scale with a low input of silica shows a variable, but commonly high content of phosphorus, indicating the iron was phosphoric.

On a broader scale, there are very few assemblages of similar medieval date in the region for comparison of the macroscopic residue assemblage (a medieval smithing hearth was recorded from site 3/14 of the Pwllheli to Blaenau pipeline, Young 2011a; medieval smithing was recorded from Parc Cybi, Young 2019; medieval smithing residues were found at Hen Gastell, Young 2016). There are distinct similarities with the SHC assemblage from Hen Gastell where besides one large and one medium SHC (c. 1000g, 306g), there was a range of small examples (72g, 80g, 84g, 104g and 168g similar to those in the present assemblage. These included one attached to an inclined second mass of slag. The Hen Gastell assemblage was also noted to contain a 'large proportion of nubs and fragments of gravelly slag'. Whilst far from conclusive, the observations suggest that the present assemblage and that from Hen Gastell may lie within the same technological milieu.

Two sites with the region have had hammerscale assemblages investigated previously: Parc Cybi (Young 2018; with three assemblages, of Roman, medieval and post-medieval age) and Hen Gastell (Young 2016; of medieval age).

The medieval phases of both these sites produce evidence for the use of iron with both elevated phosphorus (both in the iron and in the slag inclusions) and manganese (in the slag inclusions), suggesting the working of iron produced from a sedimentary ironstone source, probably a bog iron ore.

At Hen Gastell, the microresidues occurred in contexts from throughout the lifetime of the site during the 11th and 12th centuries. That assemblage may, therefore, be just slightly older than the present one.

The upper-crust normalised REE profiles for the macroresidues are similar to those recorded for the macroresidues from Hen Gastell (Young 2016 fig. 5a), suggesting that the clays employed for the hearths were similar.

If the macroscopic slags provide similarities with the assemblage from Hen Gastell, there are some significant differences in the details of the composition of the microresidues. At Hen Gastell there was a discrete population of SHS particles with around 20-25% SiO₂ that show elevated MnO (0.45-0.60%; Young 2016, fig 6). These were interpreted as having their origin in the expulsion of melted inclusions of smelting slag from the iron. Particles high in P₂O₅ occurred in the same compositional range (18-26% SiO₂ for particles with over 0.8% P₂O₅), although in a wider range of individual particles. This pattern was interpreted as evidence for the working of phosphoric iron, bearing inclusions rich in manganese and phosphorus from the smelting of the iron from a bog iron ore.

The population of SHS from the medieval ironworking in Area E at Parc Cybi showed two even more extreme SHS particles with outlying compositions at 13.5% and 18.5% SiO₂, 4.9% and 6.3% MnO and 1.5% and 2.8% P₂O₅ respectively. This provides even stronger evidence for the nature of smelting slag inclusions in the metal there.

At Llanfairfechan the pattern of these elements is different. Manganese appears at elevated levels in just a few particles in this silica range (18-25%) but phosphorus is only shown in very elevated levels in particles with less than 10% silica. Similarly, the highest level of manganese (1.4%) was recorded in a FHS particle with very low (0.57%) silica.

At Hen Gastell, it was noted (Young 2016, 9) that one of the tabular particles showed an abnormally high content of magnesium (1.05-1.83% MgO), but that was not able to be explained. At Llanfairfechan it was also the case that some of the low-silica particles (5 of the 6 SHS particles and 1 of the two FHS with the lowest SiO₂) showed an abnormally high magnesium content relative to other particles. Two of these SHS particles were also those with the high P₂O₅ contents.

The datasets from all these sites are very small and thus any comparison must only be tentative, but it is possible that the smiths at Hen Gastell relied on a higher level of fluxing. It is also possible, but extremely speculative, that more of the phosphorus was contained in the slag inclusions in the iron used at Hen Gastell, rather than being present within the iron metal.

To return to the question that prompted the analytical phase of work – why is the flake hammerscale present at Llanfairfechan in such unusually large pieces; it is not possible to answer this conclusively, but a relatively sparse use of quartz smithing flux and detachment promoted instead by phosphorus in the inner slag, may be implicated.

Discussion

The analyses suggests that the iron being worked at Llanfairfechan was phosphoric and likely to have been smelted from a bog iron ore. As such, it resembles the evidence from Parc Cybi Area E and Hen Gastell.

The three sites differ, however, in the details of the composition of the hammerscale in ways which are likely to reflect the way in which the iron was being worked rather than the raw materials. At Llanfairfechan 25% of the analysed SHS particles show SiO_2 at less than 5%, as were 10 of the 11 pieces of FHS. In contrast, at Hen Gastell no SHS particles had less than 5% SiO_2 , whereas 54% of SHS particles at Parc Cybi Area E had less than 5% SiO_2 . The iron-rich SHS particles at Parc Cybi Area E commonly showed evidence for the transfer of incompletely melted wustite into the scale, whereas evidence for this was largely lacking at Llanfairfechan (although there was evidence for the transfer of unmelted fragments of unmelted scale).

The ironworking at Llanfairfechan thus appears to have been undertaken at higher temperature than at Parc Cybi, but with a relatively low use of flux. This may have been because the iron could be welded with little or no flux. The degree to which flux was employed may well have also been an individual trait of the smith involved.

Even if its use was more restricted at Llanfairfechan, a quartz flux was clearly used. This, together with the evidence for high temperature working, indicates that welding was a part of the work undertaken in the hearth.

The hearth, therefore, cannot simply have been for a farrier or for other very light work.

Attempting to estimate what the hearth might have been used for is difficult, because of the very small assemblage of SHCs preserved – which may not necessarily be representative. If, however, the preserved single SHC at 128g is representative, then using the range of 50%-55% of that being iron lost to the hearth, then that equates to losing 65-70g of iron to the slag in a work period (this excludes iron lost to hammerscale).

Iron losses depend on many factors, but Soullignac and Serneels (2014) in an investigation into the fabrication of a simple hoe using traditional techniques, demonstrated losses of approximately 200g (+/-40g) for an SHC of this weight. If the task involved welding, then losses of approximately 20-25% were incurred in an operation involving a single weld. To generalise their results very crudely only around half the iron loss appears to have been into the slag. On this basis, around 130-140g of iron lost in total (within extremely large margins of error). Thus, perhaps the 128g SHC represents the working of 500-700g of iron into an artefact(s) weighing 350-550g (or less if multiple welds were involved).

Such a calculation is fraught with many potential sources of error and should only be used to give a most general idea of the amount of iron being processed.

Figure captions

Figure 1 upper crust-normalised rare earth element (REE) profiles (normalisation after Taylor & McLennan 1981) for a sample of hearth ceramic (LFF3) from context (7305) <7309>/<7312> and for a sample (LFF4) through the thickness of a 125g SHC from context (1603) <1605>

Figure 2. Backscattered electron image montage for sample LFF1 of spheroidal hammer scale (SHS) sub-sampled from <7311> (7305).

Figure 3. Backscattered electron images of selected grains of spheroidal hammer scale (SHS) illustrating textures across a range of iron contents. Scale bars 1mm for the whole grain images and 100µm for the microstructural detail.

S9: 0.4% SiO₂, 94.9% FeO (Group SHS (1))
 S15: 8.3% SiO₂, 85.4% FeO (Group SHS (1))
 S26: 14.1% SiO₂, 79.4% FeO (Group SHS (2))
 S1: 21.7% SiO₂, 69.8% FeO (Group SHS (2))

Figure 4. Backscattered electron image montage for sample LFF2 of tabular particles sub-sampled from from <7311> (7305). The particles are of flake hammer scale (FHS) except for T10, which is of slag.

Figure 5. Backscattered electron images of selected tabular grains illustrating the six microstructural groups. Types 1-5 are flake hammer scale (FHS); Type 6 is a slag. Scale bars are 250µm.

Figure 6. Analyses of materials from Llanfairfechan plotted within the ternary system SiO₂-Al₂O₃-FeO (fields after Schairer and Yagi 1952, fig 6).

Figure 7. Analyses of materials from Llanfairfechan plotted as:

- a. CaO + K₂O (wt%) against SiO₂ wt%
- b. P₂O₅ (wt%) against SiO₂ wt%
- c. MnO (wt%) against SiO₂ wt%
- d. SiO₂/Al₂O₃ (wt%) against SiO₂ wt%

Figure 8. Analyses of materials from Llanfairfechan plotted as:

- a. CaO + K₂O (wt%) against FeO wt%
- b. P₂O₅ (wt%) against FeO wt%
- c. MnO (wt%) against FeO wt%
- d. SiO₂/Al₂O₃ (wt%) against FeO wt%

References

JARVIS, I. & JARVIS, K. E., 1992a. Inductively coupled plasma-atomic emission spectrometry in exploration geochemistry. In: Hall, G. E. M. & Vaughlin, B. (eds), *Analytical Methods in Geochemical Exploration*. Journal of Geochemical Exploration Special Issue.

JARVIS, I. & JARVIS, K. E., 1992b. Plasma spectrometry in earth sciences: techniques, applications and future trends. In: Jarvis, I. & Jarvis, K. E. (eds), *Plasma Spectrometry in Earth Sciences*. *Chemical Geology*. **95**, 1 - 33.

PEARCE, T. J., BESLY B. M., WRAY D., & WRIGHT D. K. 1999. Chemostratigraphy: a method to improve interwell correlation in barren sequences - a case study using onshore Duckmantian/Stephanian sequences (West Midlands, UK). *Sedimentary Geology* **124**, 197- 220.

SCHAIRER, J.F. & YAGI, K. 1952. The system FeO-Al₂O₃-SiO₂. *American Journal of Science (Bowen volume)*, 471-512.

SOULIGNAC, R & SERNEELS, V. 2014. The reconstruction of smithing activities through an ethnoarchaeological and archaeometric approach of metallic wastes, pp. 277-284 in: B. Cech and T Rehren (eds) *Early Iron in Europe*, Montagnac.

TAYLOR, S.R. & McLENNAN, S.M. 1981. The composition and evolution of the continental crust: rare earth element evidence from sedimentary rocks. *Philosophical Transactions of the Royal Society*, **A301**, 381-399.

YOUNG, T.P. 2011a. Assessment of the archaeometallurgical residues from the Pwllheli to Blaenau pipeline (G2148). *GeoArch Report 2011/38*. 3 pp.

YOUNG, T.P. 2011b. Some preliminary observations on hammerscale and its implications for understanding welding. *Historical Metallurgy*, **45**, 1, 26-41.

YOUNG, T.P. 2016. Archaeometallurgical residues from Hen Gastell, Llanwnda, Gwynedd. *GeoArch Report 2016/37*. 97pp.

YOUNG, T.P. 2019. Archaeometallurgical residues from Parc Cybi, Holyhead, Ynys Môn. *GeoArch Report 2018/26*, 263pp.

YOUNG T.P., 2024. Assessment of archaeometallurgical materials from Llanfairfechan (G2495). *GeoArch Report 2024/19*, 5pp.

Table 1: summary catalogue, weights in g, assm = assemblage of small pieces.

TP	context	find	bag label	bag wt.	item wt.	item no.	description
TP16	1602	1606			6.92	1	fragment of thin dense sheet, top smooth, but slightly lobed and hints of broad dimples, base finely fuel dimpled, dense slag
					2.6	1	apparently very viscous prill of highly vesicular lining slag; maroon surface to glass dark with sand grains
TP16	1603	1605	slag		166	1	double SHC; upper. 50x90x20mm, SHC, possibly deformed by folding, attached to lower SHC, 35x60x15mm; inclined in such a way that the two are continuous on one side; base finely prilly with fuel impressions and rust; top smoothish, dimpled with faint hint of lobes only
					128	1	60x70x30mm, small dense SHC; crudely plano-convex; top with fine fuel impressions on a poorly lobate surface, partly obscured by rust; base also crudely lobate, but rusty, with abundant adhering flake hammerscale, internally vesicular, but fracture obscured partly by rust
					32	1	lobate piece of slag; low density; some gravel, but resembles the slags in the SHCs
					72	5	lower density slags - lining slags, coarsely sandy clinkery slags, maroon surface, in rounded and more sheet-like forms
					7	assm	bag with small fines sample - dust and charcoal
TP73	7302	7304	slag		7.02	1	small fragment of rather sintery-appearing slag; finely granular and rich in very fine charcoal debris
TP73	7303	7305			8.27	1	vitrified and slagged oxidised-fired lining
					7.06	2	nubs of fuel ash slag
					12.8	1	small sheet of dense slag, smooth top, fuel dimpled base; must be a modified small flow
					68	2	highly altered iron-bearing slag?
TP73	7305	7309	burnt clay, slag, charcoal	584	132	9	fragments of fired clay, all oxidised-fired with dark glassy slag; of identical aspect to b/h piece
					36	1	tip of clay around protruding blow-hole; slagged and vitrified; blow-hole slightly deformed, originally c25mm diameter? blow-hole partly occluded by slag descending across it
					24	1	slagged and vitrified oxidised-fired clay; one side shows a pale curved lateral face suggests a tuyère margin
					352	16	Iron slag; of the two largest pieces, each 64g, one shows lobate flow across hearth floor, the other may be a proto-SHC; other fragments very variable - the denser slags tend to be fragments of sheets, lower density ones tend to be more blebby and lobate
					8	assm	small bag labelled 'iron rich material from soil' which includes slag debris and hammerscale

TP73	7305	7311	slag/hammerscale from <5>	360	360	assm	unusual assemblage with very large, very shiny FHS fragments; lots of spheroids and rounded blebs, many of maroon-surfaced FAS/lining slag; some fired clay; some probably oxidised iron debris in thin sheets and some blebby pieces of dense slag, but these are rarer
TP73	7305	7312	slag from coarse residue <5>	140	3.96	1	fiddle key nail
					61.6	27	blebby low-density slags
					15.61	8	oxidised-fired clay
					0.72	1	slagged oxidised-fired clay - possibly from blow-hole margin
					0.66	1	slagged oxidised-fired clay
					16.65	4	probable scraps of iron
					16.55	3	laminated iron cemented sand; has rounded cavities, but does not appear to be a slag
					8.74	4	rounded pebbles of natural rock
					6.92	4	dense slag, mostly finely prilly
					5.51	1	laminated sandy material with charcoal clast
TP75	7505	75131	furnace lining		4.67	1	small fragment of fired clay, oxidised in core, reduced on surface; front face is 14x24mm, then turns to side 12mm high, along a line with a radius of 30mm (but angular so this estimate is only approximate); could be from the margin of the face of a tuyère
TP40	4002	4004			11.27	1	lining slag with small amount of attached vitrified lining; slag surface shows some deep dimples and a slightly pendent lobe?
TP129	12903	12907	mag material from <8>	92	92	assm	assemblage with much concretionary material; one fragment appears to be plaster with moulds of organic temper; there are fragments of burnt organic material, and some of very fine clinker with globules on millimetre scale forming agglomerations, other concretionary materials may be natural Fe/Mn crusts; one piece appears to be sandstone grain from inside coal seam and another is possibly a sphaerosiderite grain; the magnetic nature of the now-pinkish shale, that dominates, probably suggests this is partly burnt, however, the intergrowth of Mn oxides and what appears to be fired clay, may suggest that some of the colour is natural.

Table 2: major element analyses by XRF expressed as wt% for macroscopic materials. Raw measured values, except for calculated columns for FeO (as an alternative to Fe₂O₃). < = below detection.

Sample	SiO ₂	Al ₂ O ₃	Fe ₂ O ₃	FeO	MnO	MgO	CaO	Na ₂ O	K ₂ O	TiO ₂	P ₂ O ₅	SO ₃	LOI	total
LFF3	50.33	19.19	19.63	17.66	0.253	2.26	0.46	0.671	2.814	1.002	0.173	<0.15	4.36	96.78
LFF4	18.68	4.73	76.18	68.55	0.147	1.29	0.83	<0.1	0.807	0.384	0.271	0.251	-2.09	103.32

Table 3: trace element analyses by ICP-MS for macroscopic materials (part 1). Raw numerical values in ppm. < = below detection.

Sample	Be	V	Cr	Co	Ni	Cu	Zn	Ga	Rb	Sr	Y	Zr	Nb	Mo	Sn	Cs	Ba
LFF3	2.90	144.95	101.12	24.22	63.44	136.26	113.67	25.09	128.82	73.49	25.60	118.54	14.57	3.15	6.60	6.88	534.13
LFF4	0.71	38.24	27.56	19.94	42.69	108.78	<	7.99	21.87	76.25	9.96	79.92	4.53	9.23	14.52	0.47	200.16

Table 4: trace element analyses by ICP-MS for macroscopic materials (part 2). Raw numerical values in ppm. < = below detection.

Sample	La	Ce	Pr	Nd	Sm	Eu	Gd	Tb	Dy	Ho	Er	Tm	Yb	Lu	Hf	Ta	W	Pb	Th	U
LFF3	32.40	70.15	7.68	28.29	5.19	1.07	4.53	0.73	4.77	0.96	2.87	0.43	2.86	0.43	3.35	1.11	1.55	28.20	12.58	2.36
LFF4	9.03	19.14	2.28	8.72	2.01	0.42	1.89	0.30	1.95	0.40	1.17	0.16	1.12	0.17	2.22	0.31	0.27	1.58	2.98	0.73

Table 5: estimated major element composition expressed as wt% for SHS particles (LFF1) ordered by SiO₂ content. For details of how these were calculated see text. < = below detection.

Particle#	Na ₂ O	MgO	Al ₂ O ₃	SiO ₂	P ₂ O ₅	SO ₃	Cl	K ₂ O	CaO	TiO ₂	V ₂ O ₅	Cr ₂ O ₃	MnO	FeO	CoO	NiO
<i>Normal</i>																
S14	<	<	1.24	4.71	0.33	<	<	<	0.16	<	<	<	0.15	92.93	0.48	<
S28	<	0.10	1.94	7.05	0.30	<	<	<	0.20	<	<	<	0.19	89.72	0.50	<
S2	<	0.20	2.67	7.18	0.21	<	<	<	0.15	<	<	<	0.06	89.10	0.43	<
S27	<	0.44	2.61	8.75	0.21	<	<	<	0.22	0.15	<	<	0.15	86.86	0.62	<
S6	0.15	0.39	2.39	10.28	0.30	<	<	0.20	0.21	0.21	<	<	<	85.43	0.46	<
S7	<	0.52	2.52	11.90	0.31	<	<	<	0.54	0.18	<	<	0.06	83.51	0.45	0.03
S3	0.11	0.68	3.34	13.26	0.08	<	<	0.25	0.26	0.30	<	<	0.13	81.17	0.41	<
S25	<	0.67	2.14	13.97	0.39	<	<	<	0.41	0.27	<	<	0.18	81.48	0.47	<
S13	<	0.18	1.42	13.97	<	<	<	0.20	0.18	<	<	<	<	83.58	0.47	<
S16	<	0.40	1.51	14.18	0.29	<	<	<	0.41	0.07	<	<	0.23	82.48	0.42	<
S26	0.33	0.35	2.45	14.70	0.43	<	<	0.70	0.99	0.09	<	<	0.19	79.35	0.42	<
S19	0.40	0.30	2.63	15.37	0.17	<	<	0.70	0.47	0.17	<	<	0.11	79.22	0.46	<
S32	<	0.67	2.52	15.94	0.48	<	<	<	0.99	0.16	<	<	0.68	78.14	0.41	<
S24	<	0.79	1.92	16.05	0.27	<	<	<	0.26	0.41	<	<	<	79.80	0.50	<
S29	0.87	0.71	4.43	16.38	0.27	<	<	1.32	1.55	0.24	<	<	0.14	73.61	0.42	<
S10	0.09	0.67	2.45	18.75	0.58	<	<	0.31	0.59	0.20	<	<	0.10	75.85	0.41	<
S31	<	0.90	2.67	19.92	0.37	<	<	0.21	0.63	0.37	<	<	<	74.45	0.46	<
S21	0.24	0.70	5.34	20.67	0.71	<	<	0.82	0.91	0.37	<	<	0.49	69.34	0.38	<
S22	0.51	0.62	4.55	20.87	0.62	<	<	1.19	1.51	0.32	<	<	0.16	69.30	0.34	<
S23	0.43	0.54	4.16	21.63	0.59	<	<	1.26	0.67	0.29	<	<	0.33	69.73	0.37	<
S18	0.78	1.03	5.32	21.64	0.39	<	<	1.22	1.71	0.37	<	<	0.22	66.92	0.39	<
S1	0.37	0.78	4.64	21.72	0.27	<	<	0.89	0.63	0.39	<	<	0.17	69.77	0.36	<
<i>Slightly suspect</i>																
S8	<	0.27	3.37	5.70	0.68	<	<	0.15	0.30	<	<	<	<	87.32	0.95	<
S15	0.13	0.46	4.20	8.29	0.32	<	<	0.24	0.33	0.15	<	<	<	85.42	0.47	<
<i>Very suspect</i>																
S9	<	0.08	3.89	0.41	0.07	<	<	<	0.15	<	<	<	<	94.86	0.49	0.05
S17	<	0.15	8.66	0.87	0.12	<	<	<	0.12	0.05	<	<	<	89.55	0.49	<
s4	<	0.48	6.97	1.40	1.80	0.17	<	<	0.19	0.18	<	<	0.14	88.20	0.47	<
S30	<	<	10.45	1.67	0.39	0.09	<	0.06	0.30	<	<	<	0.06	86.49	0.48	<
S11	<	0.82	7.05	2.21	1.26	0.67	<	<	0.24	0.60	<	<	0.18	86.52	0.47	<
S5	0.11	0.55	8.34	2.95	0.15	0.26	<	0.11	0.45	0.23	<	<	<	86.32	0.47	0.02
S12	<	0.21	3.82	3.01	0.16	<	<	0.04	0.09	<	<	<	0.23	91.97	0.49	<

Table 6: physical and mineralogical properties of spheroidal hammerscale particles (LFF1). Ordered by SiO₂ content.

Particle#	SiO ₂ wt%	main porosity	microstructure	quartz grains	metal prills	unmelted scale	group
							1
S9	0.41	dispersed	stout wustite dendrites and pseudo-dendrites				1
S17	0.87	central	stout wustite dendrites, but variable size		y		1
S4	1.40	dispersed	stout wustite dendrites, but variable size				1
S30	1.67	central	stout wustite dendrites, but variable size				1
S11	2.21	central	finely dendritic wustite in glass – nucleated on emulsion blebs?				1
S5	2.95	central	stout wustite dendrites, but variable size		?	y?	1
S12	3.01	central	initial magnetite dendrites followed by dense but fine and well-formed wustite				1
S14	4.71	central	stout wustite dendrites and pseudo-dendrites in fayalite				1
S8	5.70	marginal	initial magnetite dendrites followed by dense but fine and well-formed wustite				1
S28	7.05	dispersed	stout wustite dendrites, but variable size			y	1
S2	7.18	dispersed	stout wustite dendrites		?		1
S15	8.29	dispersed	stout wustite dendrites, but variable size, in glass				1
S27	8.75	central	medium wustite in glass				1
S6	10.28	central	stout wustite dendrites in glass				1
S7	11.90	dispersed	fine wustite dendrites in low proportion of glass	400µm grain		y	1
S3	13.26	dispersed	finely dendritic wustite in glass		?		1
S25	13.97	central	finely dendritic wustite in fayalite	50µm grain		y	1
S13	13.97	central	fine-medium wustite in fayalite				1
S16	14.18	dispersed	finely dendritic wustite in fayalite	80µm grain		y	1
S26	14.70	dispersed	fine-medium wustite in fayalite/glass	300µm grain			2
S19	15.37	dispersed	initial magnetite dendrites followed by dense but fine and well-formed wustite				2
S32	15.94	dispersed	finely dendritic wustite in fayalite				2
S24	16.05	dispersed	finely dendritic wustite in fayalite/glass			y?	1
S29	16.38	dispersed	finely dendritic wustite in glass, with wustite clots				2
S10	18.75	dispersed	finely dendritic wustite in fayalite	80µm grain			2
S31	19.92	dispersed	finely dendritic wustite in fayalite				2
S21	20.67	dispersed	finely dendritic wustite in glass, with wustite clots	multiple <150µm			2
S22	20.87	dispersed	finely dendritic wustite in fayalite/glass	multiple <100µm			2
S23	21.63	central	finely dendritic wustite in fayalite/glass				2
S18	21.64	dispersed	finely dendritic wustite in fayalite/glass				2
S1	21.72	dispersed	finely dendritic wustite in glass				2
S20	n/a	central	stout wustite dendrites and pseudo-dendrites		y	y	n/a

Table 7: estimated major element analyses by EDS expressed as wt% for flake hammerscale particles (LFF2). For details of how these were calculated see text. < = below detection.

Particle#	Na ₂ O	MgO	Al ₂ O ₃	SiO ₂	P ₂ O ₅	SO ₃	Cl	K ₂ O	CaO	TiO ₂	V ₂ O ₅	Cr ₂ O ₃	MnO	FeO	CoO	NiO
<i>Normal</i>																
T9	0.36	<	0.85	3.21	1.06	<	<	0.39	0.49	<	<	<	<	92.87	0.54	0.23
T10	0.89	0.85	4.95	19.24	0.24	0.05	<	1.74	2.31	0.32	<	<	0.20	68.75	0.38	<
<i>Slightly suspect</i>																
T11	<	0.30	1.86	0.57	0.19	<	<	<	0.19	<	<	<	1.35	95.03	0.49	<
T8	0.23	0.23	3.29	4.26	0.18	<	<	0.18	0.16	<	<	<	<	90.92	0.54	<
T1	<	0.36	2.92	4.96	0.23	<	<	0.22	0.25	0.15	<	<	0.12	90.21	0.59	<
<i>Very suspect</i>																
T6	<	<	1.42	0.42	0.31	<	<	<	<	<	<	<	<	97.39	0.46	<
T12	<	<	2.71	1.58	<	<	<	<	<	<	<	<	0.28	95.02	0.41	<
T13	<	0.23	2.29	1.79	0.19	0.06	<	<	0.38	0.06	<	<	0.43	94.11	0.46	<
T2	<	0.16	4.33	1.81	0.49	<	<	0.11	0.40	<	<	<	<	92.04	0.50	<
T4	0.11	0.15	7.49	3.50	0.39	0.08	<	0.13	0.44	<	<	<	0.18	87.14	0.38	<
T3	<	0.27	2.30	3.09	1.64	0.14	<	0.23	0.88	<	<	<	0.40	90.43	0.47	0.15
T5	<	0.26	4.22	5.39	0.51	<	<	0.23	0.57	<	<	<	<	88.23	0.40	<
T7	<	0.56	5.97	6.92	0.49	<	<	<	0.49	0.14	<	<	0.27	84.75	0.42	<

Table 8: physical and mineralogical properties of flake hammerscale particles (LFF2). Ordered SiO₂ content.

particle#	SiO ₂ wt%	microstructure	iscorite?	quality
T6	0.42	1		normal
T11	0.57	2	yes	slightly suspect
T12	1.58	2	yes	very suspect
T13	1.79	3		very suspect
T2	1.81	2	yes	very suspect
T9	3.21	3		normal
T8	4.26	4		slightly suspect
T1	4.96	4		slightly suspect
T4	3.50	2		very suspect
T3	3.09	1		very suspect
T5	5.39	4		very suspect
T7	6.92	7		very suspect
T10	19.24	6		very suspect

..

Table 9: major element analyses by EDS expressed as wt% for the inner slag layer of flake hammerscale particles (LFF2). < = below detection.

Particle#	Na ₂ O	MgO	Al ₂ O ₃	SiO ₂	P ₂ O ₅	SO ₃	Cl	K ₂ O	CaO	TiO ₂	V ₂ O ₅	Cr ₂ O ₃	MnO	FeO	CoO	NiO
<i>Normal</i>																
T9	<	0.57	4.83	9.63	0.97	0.21	<	<	0.74	0.26	<	<	0.34	82.06	0.42	<
<i>Slightly suspect</i>																
T10	<	0.11	3.50	5.33	1.71	<	<	<	0.33	0.14	<	<	0.10	88.32	0.46	<

Figure 1

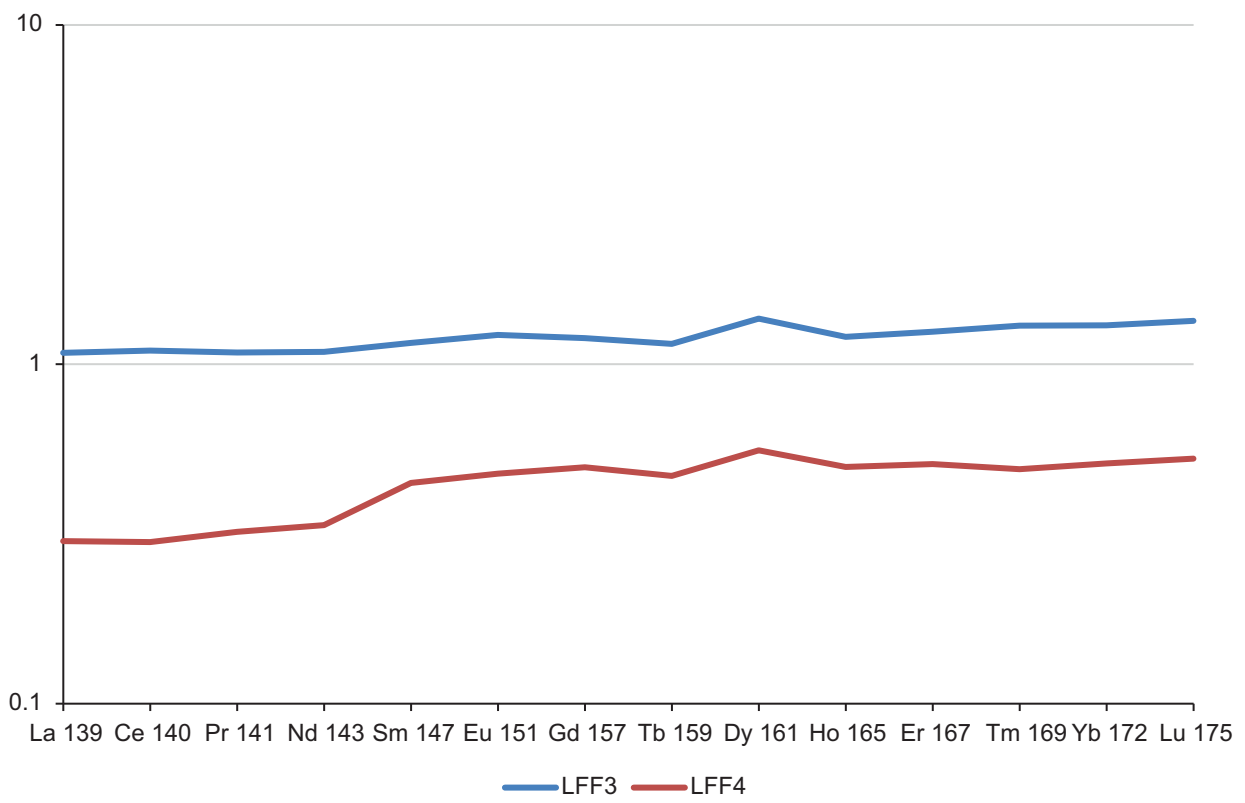


Figure 2

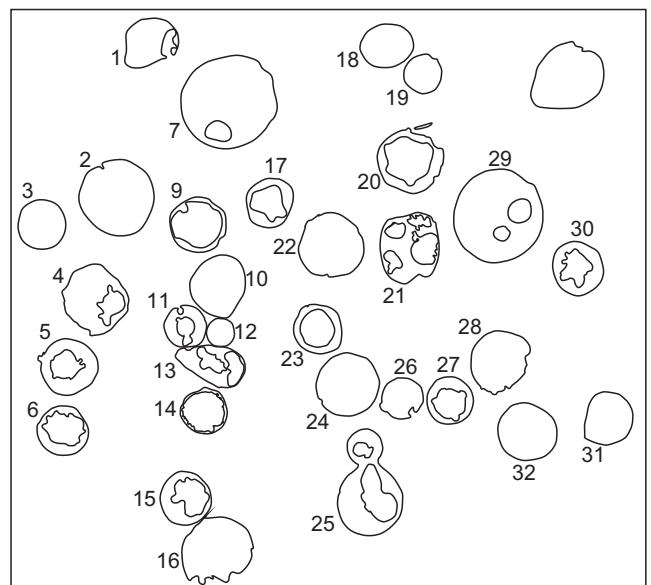
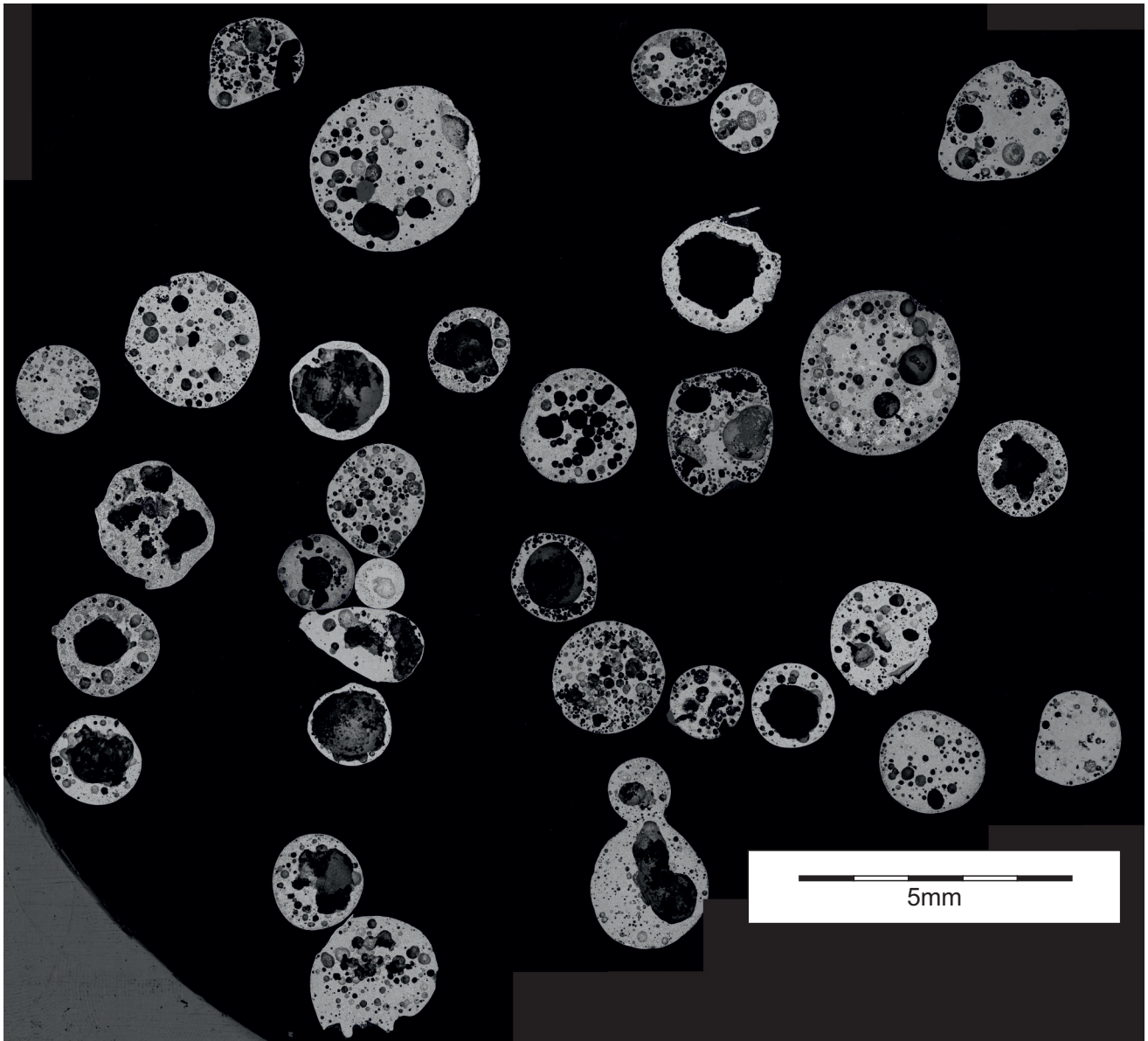


Figure 3

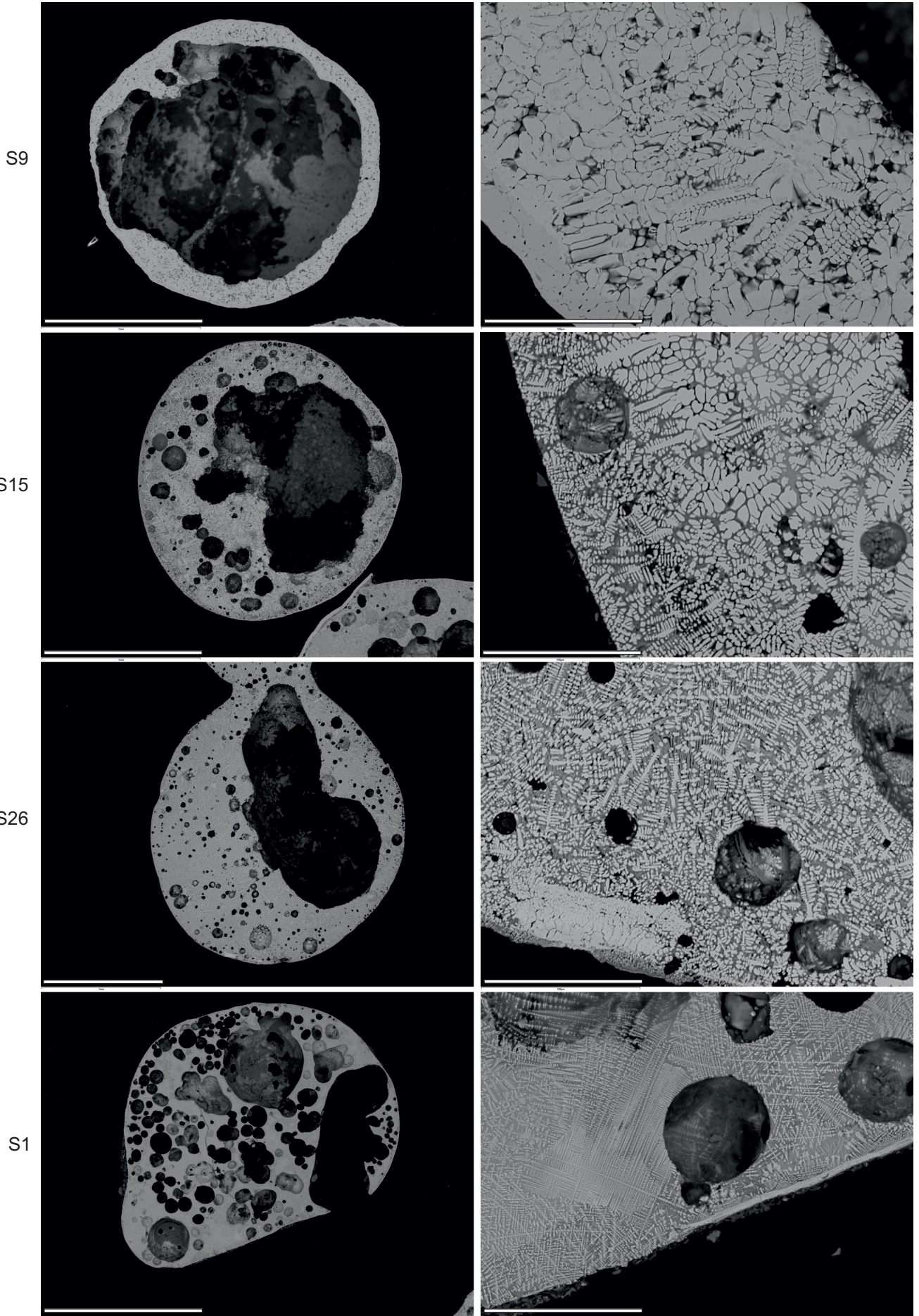
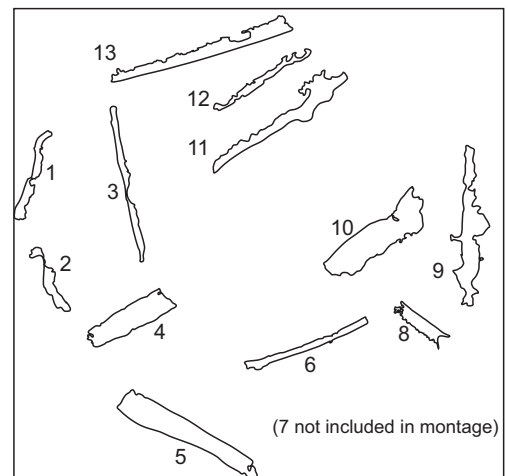
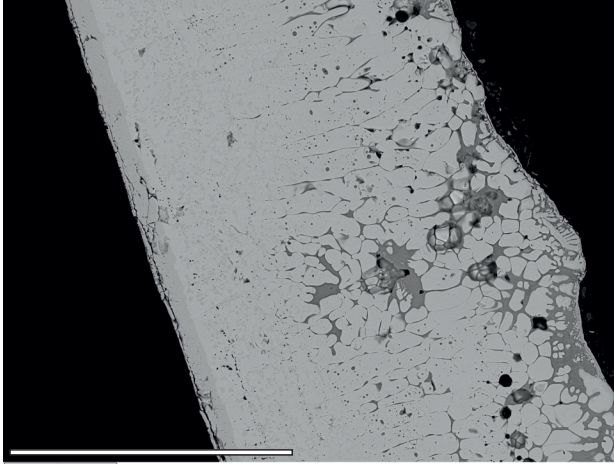


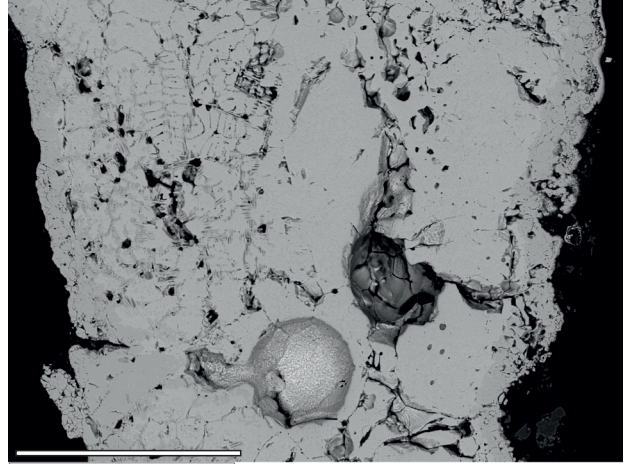
Figure 4



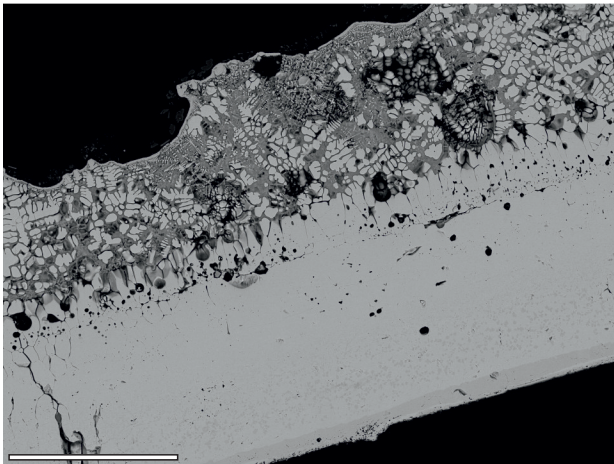
1 (T3)



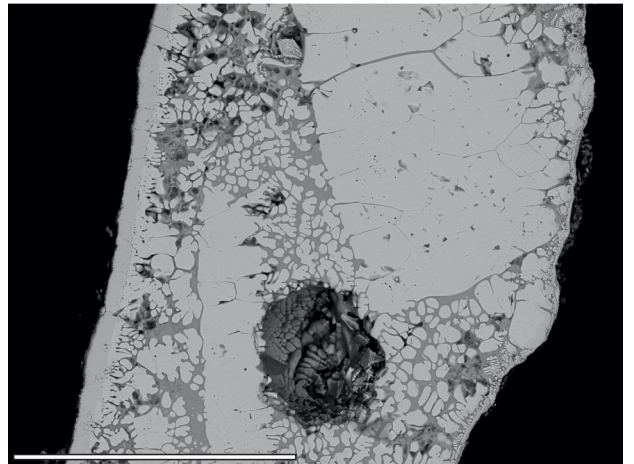
2 (T2)



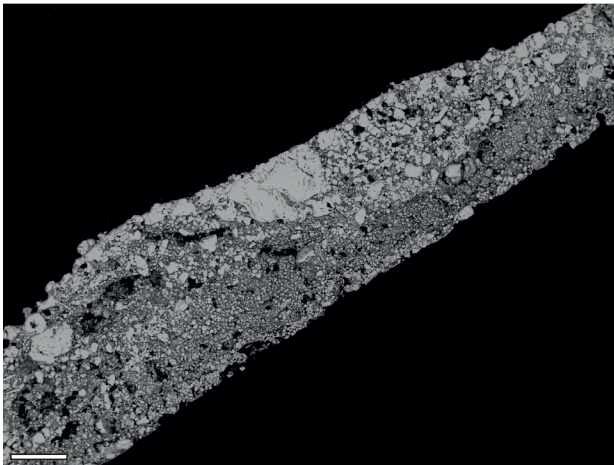
3 (T13)



4 (T1)



5 (T7)



6 (T10)

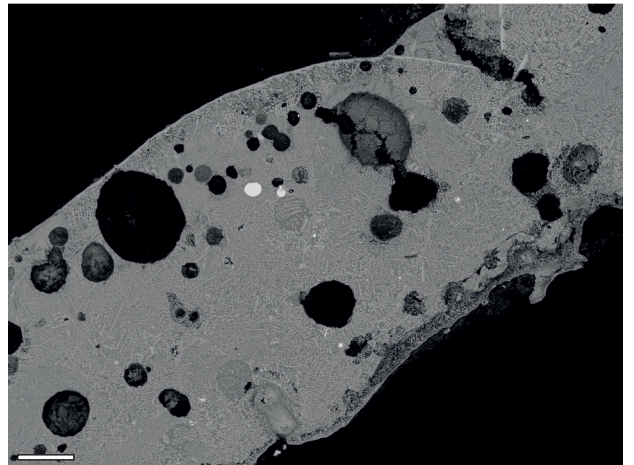


Figure 6

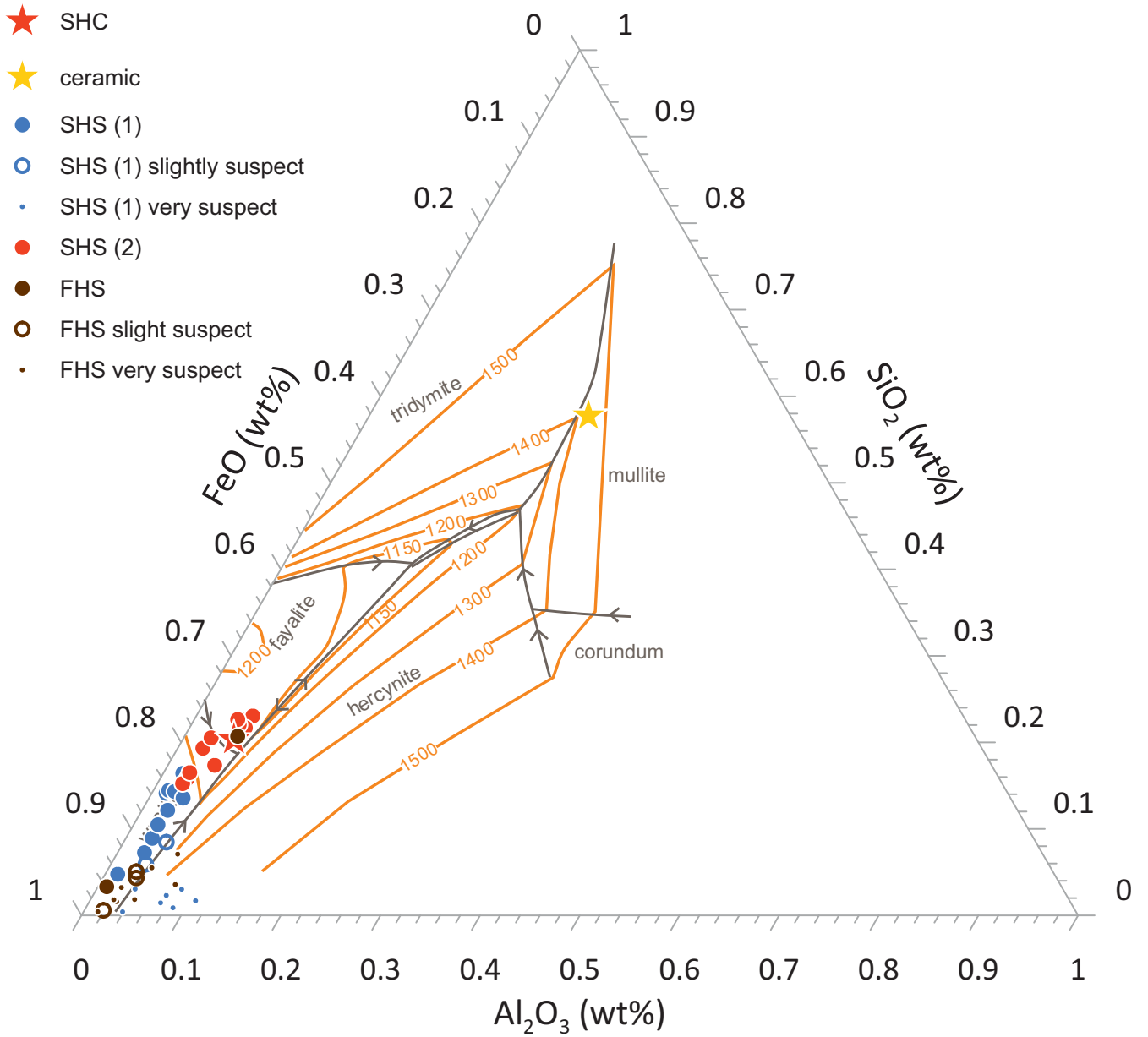


Figure 7

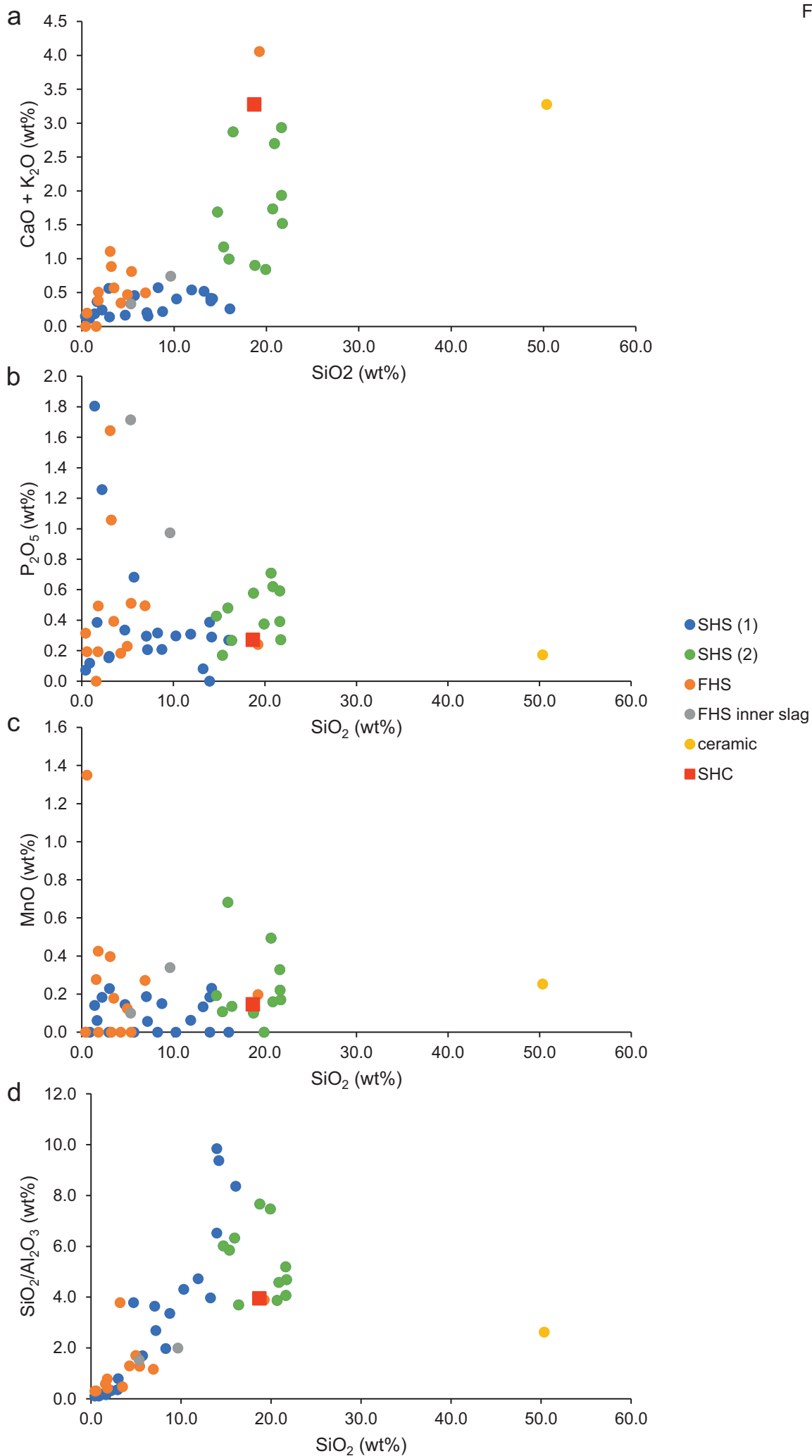
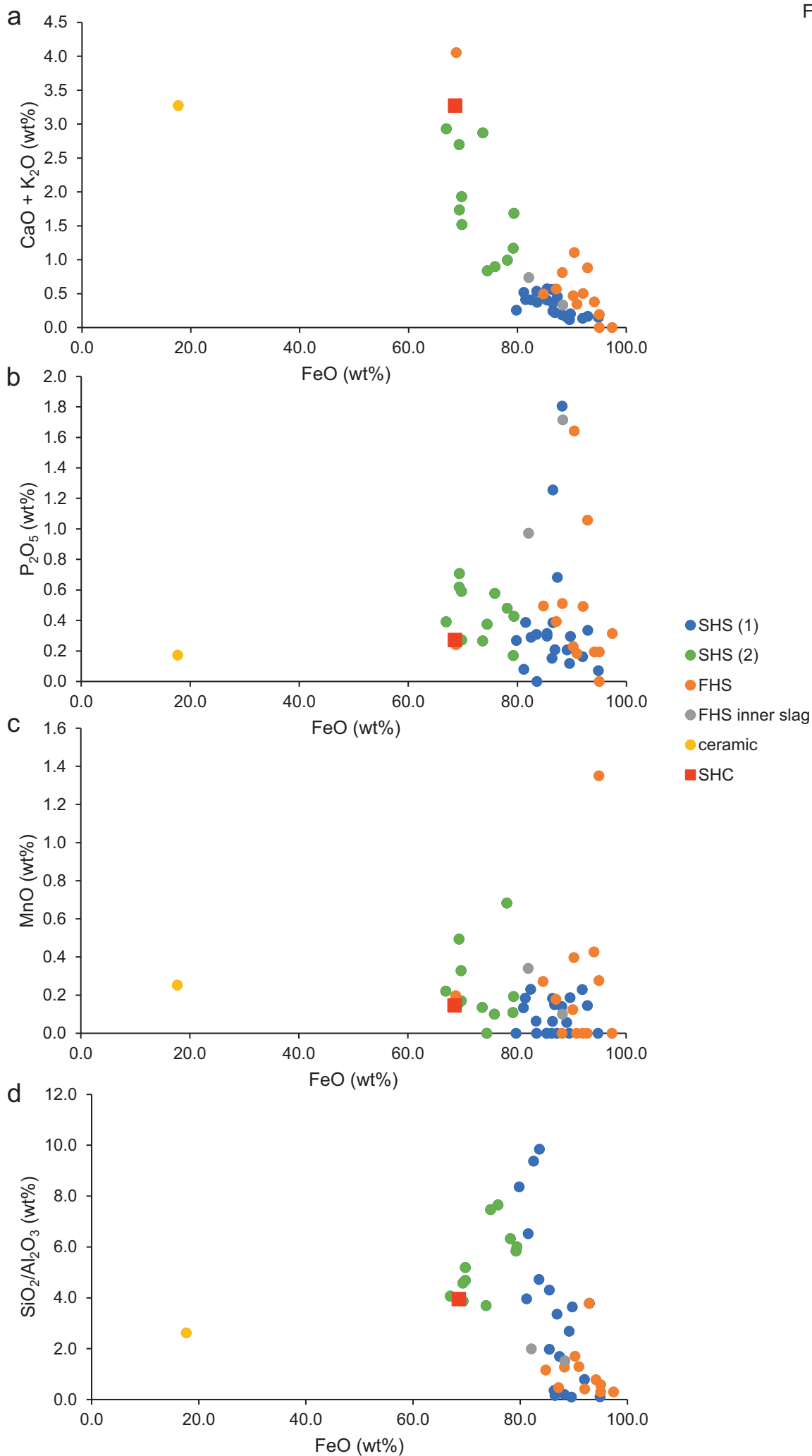


Figure 8



Ironworking residues from Llanfairfechan (G2495)
GeoArch Report 2025/01

Appendix A:

Archive of EDS analyses, presented as wt% element, collected as 'all elements measured'.

sample	site	#	O	Na	Mg	Al	Si	P	S	Cl	K	Ca	Ti	V	Cr	Mn	Fe	Co	Ni	Cu	Zn	As	Sn	Sb	Ba	Pb	Total
LFF2	15	1410	30.53	0	0.19	0.74	7.72	2.83	0.07	0	0.16	0.65	0	0	0	0.19	47.29	0.2	0	0	0	0	0	0	0	0	90.56
LFF2	15	1411	31.91	0.13	0.24	0.82	8.54	2.61	0	0	0.15	0.64	0	0	0	0.15	51.11	0.24	0	0	0	0	0	0	0	0	96.54
LFF2	15	1412	33.65	0	0.23	1.04	9.88	3	0	0	0.16	0.6	0	0	0	0.2	45.2	0.27	0	0	0	0	0	0	0	0	94.22
LFF2	15	1413	32.39	0	0.24	0.81	8.97	2.97	0	0	0.15	0.78	0.07	0	0	0.23	46	0.28	0	0	0	0	0	0	0	0	92.88
LFF2	15	1414	26.58	0	0.18	4.07	6.17	1.73	0.07	0	0	0.92	0.06	0	0	0.15	48.49	0.26	0	0	0	0	0	0	0	0	88.68
LFF2	15	1415	32.62	0	0.25	0.63	9.05	3.18	0	0	0	0.98	0	0	0	0.22	45.97	0.27	0	0	0	0	0	0	0	0	93.16
LFF2	15	1416	23.98	0	0.19	0.75	6.38	1.64	0	0	0	0.61	0	0	0	0.15	57.83	0.33	0	0	0	0	0	0	0	0	91.85
LFF2	15	1417	13.39	0.34	0.11	2.17	1.2	0.2	0.08	0.19	0.21	0.58	0.12	0	0	0	43.95	0.19	0	0	0	0	0	0	0	0	62.72
LFF2	15	1418	27.48	0	0	0.3	0	0	0	0	0.42	0.09	0	0	0	0	65.91	0.26	0	0	0	0	0	0	0	0	94.46
LFF2	15	1419	24.73	0.33	0	0.29	0	0	0	0	0	0.24	0	0	0	0	68.87	0.28	0	0	0	0	0	0	0	0	94.73
LFF2	15	1420	23.86	0	0	0.32	0.12	0	0	0	0	0	0	0	0	0	68.89	0.36	0	0	0	0	0	0	0	0	93.55
LFF2	15	1421	22.11	0	0	0.32	0.06	0	0	0	0	0	0	0	0	0	72.85	0.37	0	0	0	0	0	0	0	0	95.72
LFF2	16	1422	27.3	0.48	0.46	3.17	7.26	0.14	0.1	0	1.03	1.22	0.23	0	0	0.11	50.96	0.32	0	0	0	0	0	0	0	0	92.78
LFF2	16	1423	27.87	0.69	0.52	2.51	8.83	0.12	0.06	0	1.43	1.62	0.22	0	0	0.13	53.43	0.23	0	0	0	0	0.21	0	0	0	97.88
LFF2	16	1424	28.74	0.64	0.54	2.8	9.12	0.09	0	0	1.48	1.67	0.19	0	0	0.17	52.05	0.3	0	0	0	0	0	0	0	0	97.8
LFF2	16	1425	0	0	0	0.23	0.19	0	0	0	0	0	0	0	0	0	92.05	0.58	0	0	0	0	0	0	0	0	93.04
LFF2	16	1426	2.01	0	0	0.2	0.06	0	0.07	0	0	0	0	0	0	0	88.42	0.54	0.24	0	0	0.56	0	0	0	0	92.11
LFF2	16	1427	2.67	0	0	0.31	0.14	0	0	0	0	0	0	0	0	0	93.24	0.59	0	0	0	0	0	0	0	0	96.96
LFF2	16	1428	0	0	0	0.22	0	0	0	0	0	0.07	0	0	0	0	95.13	0.64	0	0	0	0	0	0	0	0	96.06
LFF2	16	1429	4.95	0	0.1	0.78	1.65	0	0	0	0.23	0.23	0.08	0	0	0	89.07	0.47	0	0	0	0	0	0	0	0	97.56
LFF2	17	1430	0	0	0	0.17	0	0	0	0	0	0	0	0	0	0	88.76	0.61	0.11	0	0	0	0	0	0	0	89.66
LFF2	17	1431	0	0	0	0.19	0	0	0	0	0	0	0	0	0	0	95.32	0.66	0.12	0	0	0	0	0	0	0	96.29
LFF2	17	1432	0	0	0	0.2	0	0	0	0	0	0	0	0	0	0	94.86	0.62	0.14	0	0	0	0	0	0	0	95.83
LFF2	17	1433	0	0	0	0.22	0	0	0	0	0	0	0	0	0	0	94.72	0.6	0.12	0	0	0	0	0	0	0	95.66
LFF2	17	1434	0	0	0	0.22	0	0	0	0	0	0	0	0	0	0	93.96	0.61	0	0	0	0	0	0	0	0	94.79
LFF2	17	1435	0	0	0	0.23	0	0	0	0	0	0	0	0	0	0	90.26	0.63	0.21	0	0	0.54	0	0	0	0	91.87
LFF2	17	1436	0	0	0	0.22	0	0	0	0	0	0	0	0	0	0	89.84	0.56	0.18	0	0	0.47	0	0	0	0	91.28
LFF2	17	1437	0	0	0	0.22	0	0	0	0	0	0	0	0	0	0	90.38	0.62	0.24	0	0	0.5	0	0	0	0	91.96
LFF2	17	1438	22.15	0	0.32	0.38	0.34	0	0	0	0.08	0.13	0.29	0	0	0.09	72.38	0.35	0	0	0	0	0	0	0	0	96.52
LFF2	17	1439	22.03	0	0.37	0.54	0.92	0	0	0	0.25	0.26	0.22	0	0	0.11	70.2	0.35	0	0	0	0	0	0	0	0	95.27
LFF2	17	1440	36.41	1.1	0.62	4.33	17.76	0.25	0	0	2.77	3.76	0.11	0	0	0.15	32.82	0.19	0	0	0	0	0	0	0	0	100.3
LFF2	17	1441	33.85	1.16	0.62	3.99	15.01	0.22	0	0	2.12	2.58	0.15	0	0	0.15	45.07	0.26	0	0	0	0	0	0	0	0	105.2
LFF2	17	1442	36.36	0.97	0.58	4.27	17.38	0.27	0.05	0	2.35	4.8	0.09	0	0	0.15	31.57	0.14	0	0	0	0	0	0.4	0	0	99.38
LFF2	17	1443	35.61	0.92	0.64	4.21	17.55	0.24	0.06	0	2.72	3.56	0.11	0	0	0.17	32.89	0.23	0	0	0	0	0	0	0	0	98.9
LFF2	17	1444	35.16	0.92	0.61	3.87	17.48	0.29	0.06	0	2.61	3.71	0.16	0	0	0.23	33.28	0.18	0	0	0	0	0	0.25	0	0	98.8

Ironworking residues from Llanfairfechan (G2495)
GeoArch Report 2025/01

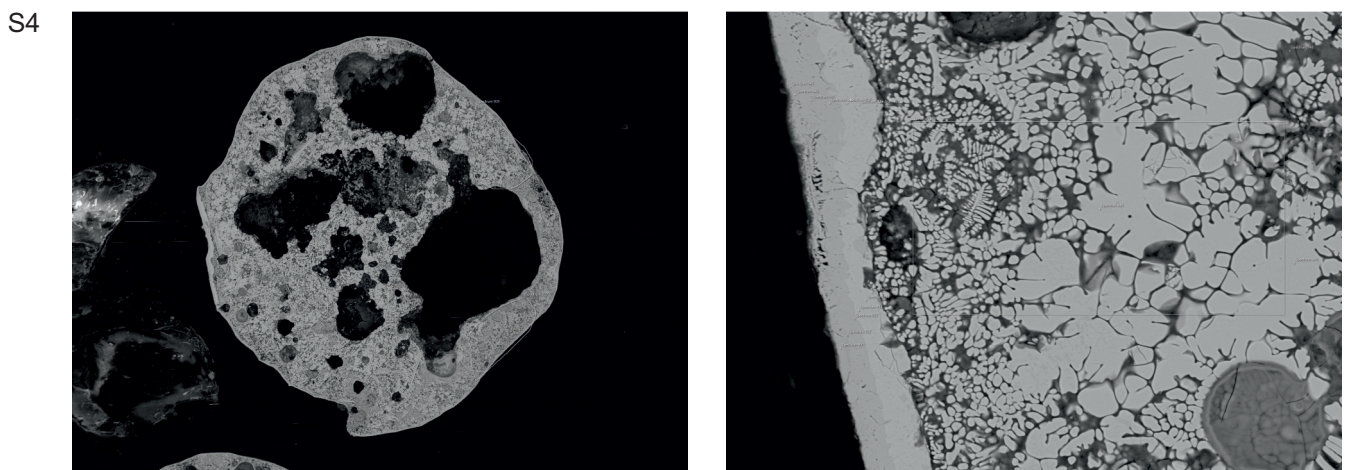
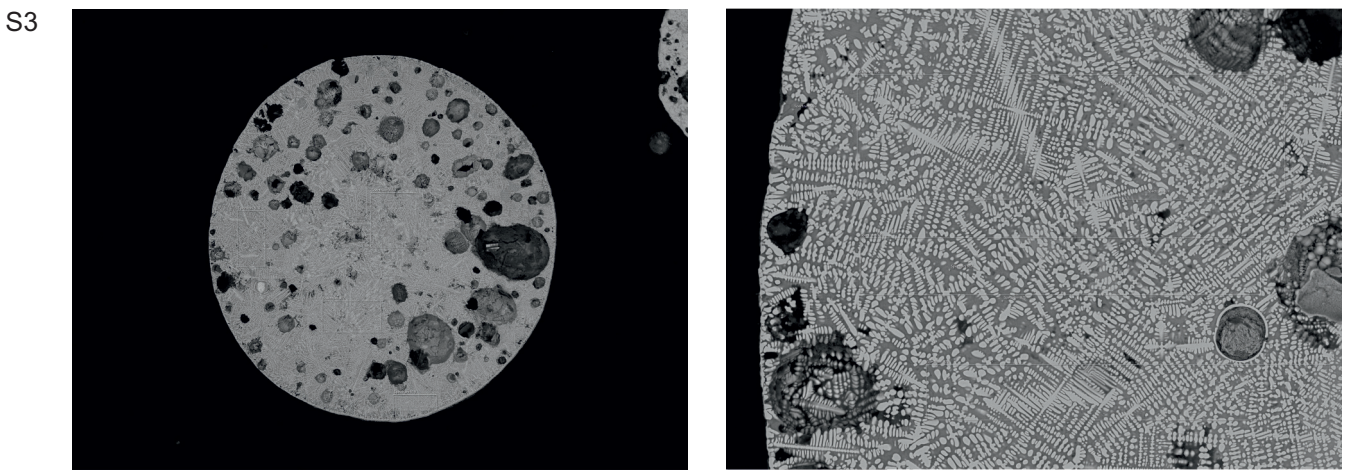
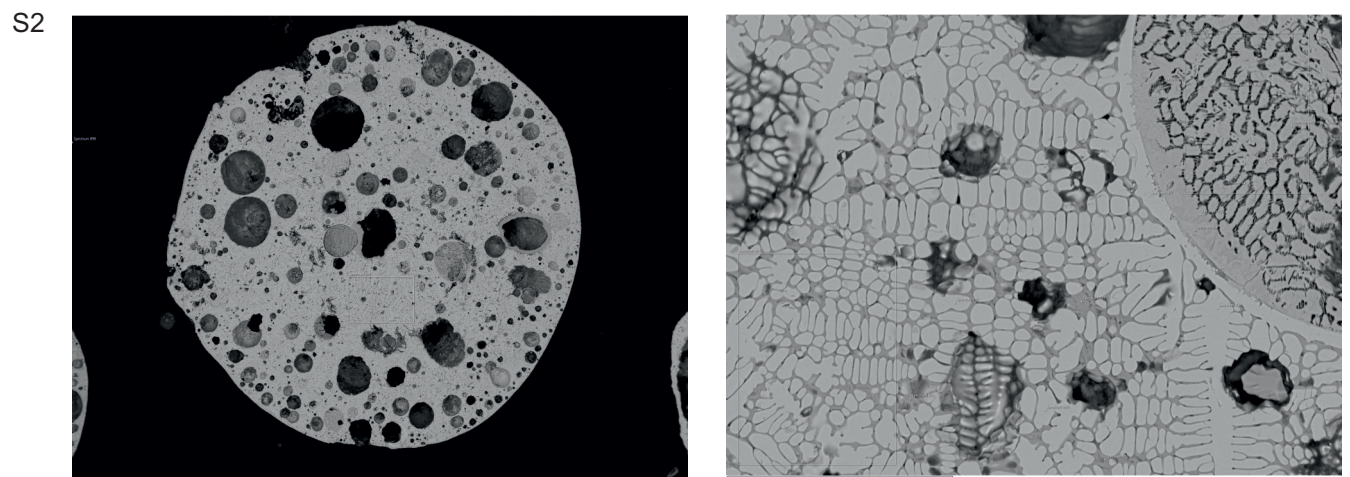
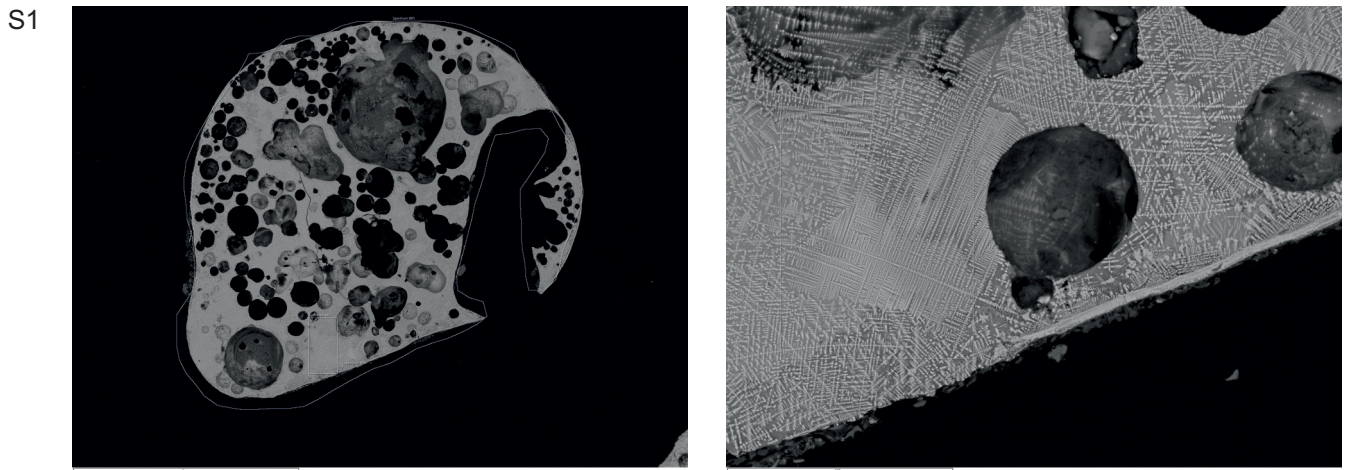
Appendix B:

Archive of BSEM images showing locations of analyses.

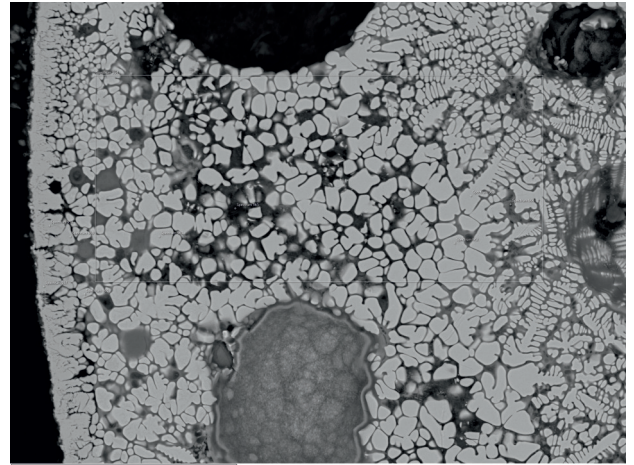
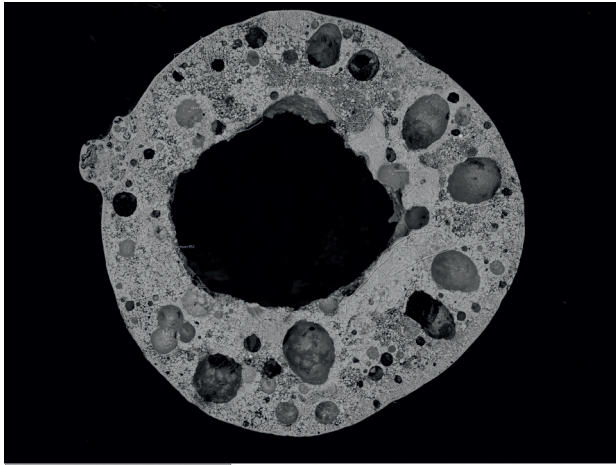
Ironworking residues from Llanfairfechan (G2495)
GeoArch Report 2025/01

Appendix B:

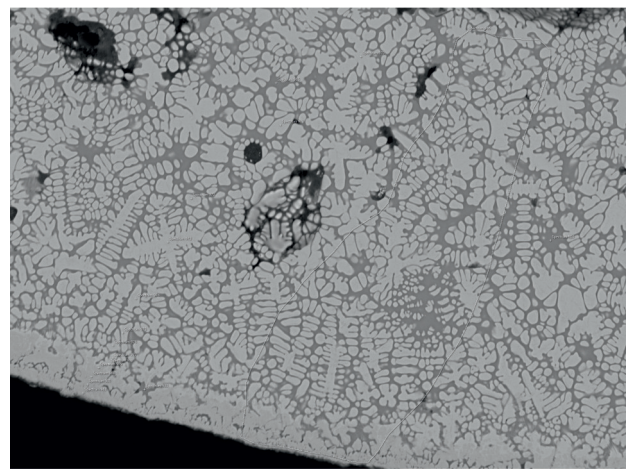
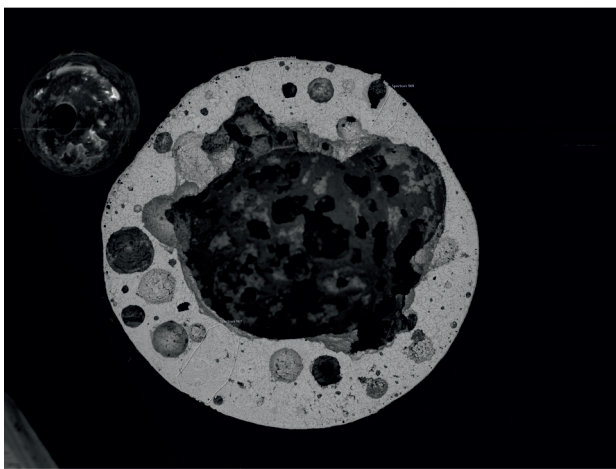
Archive of BSEM images showing locations of analyses.



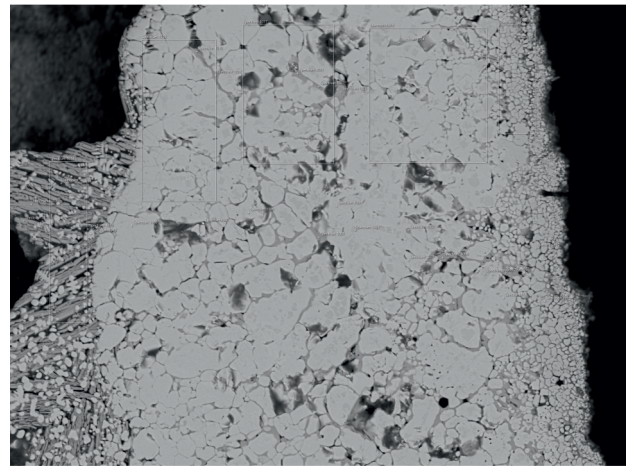
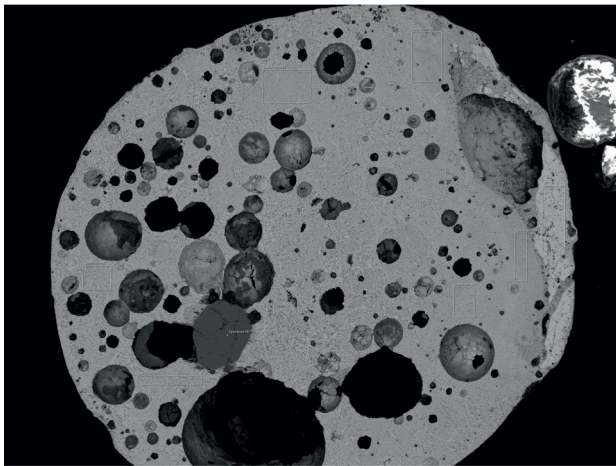
S5



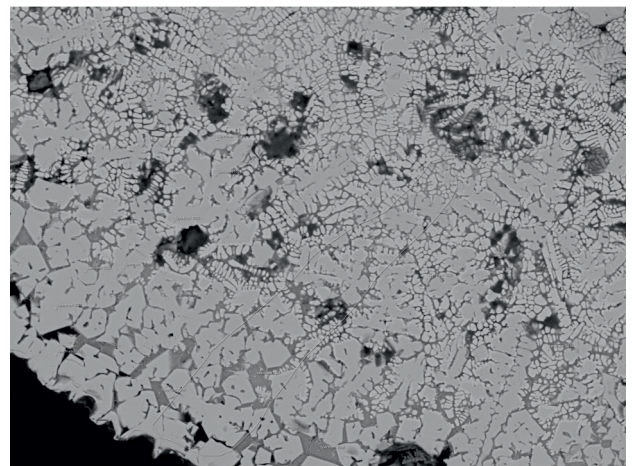
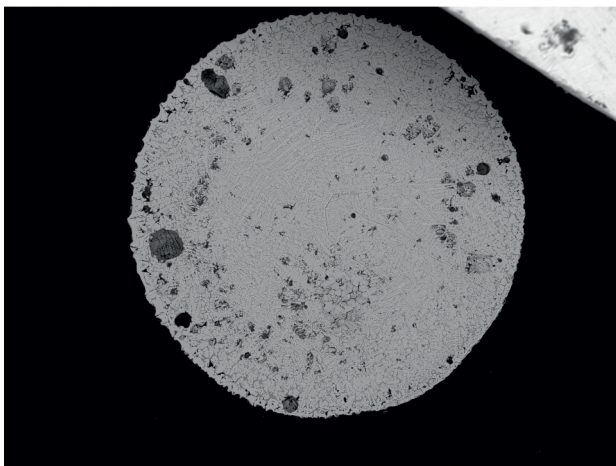
S6

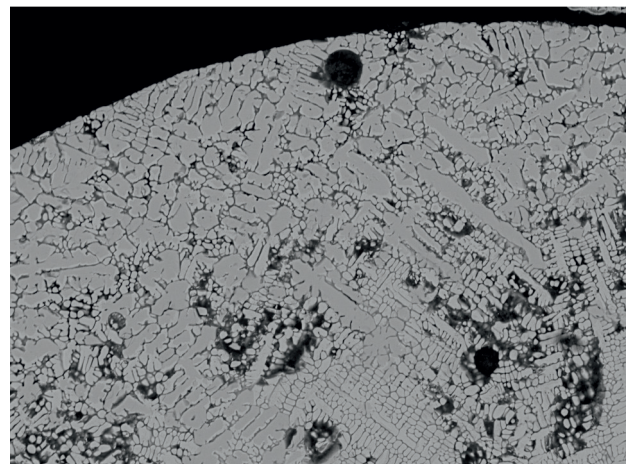
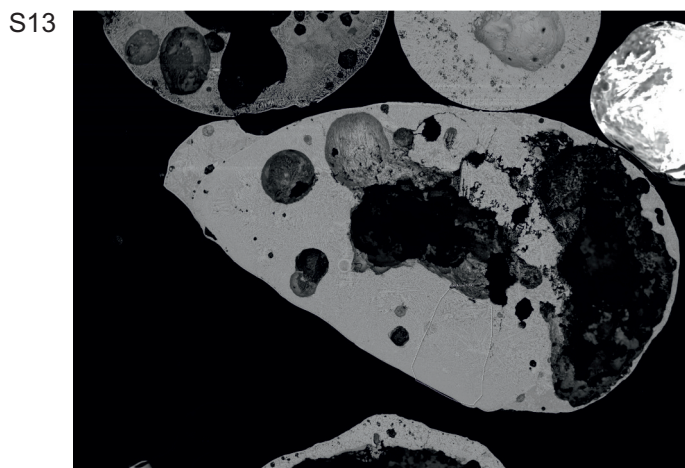
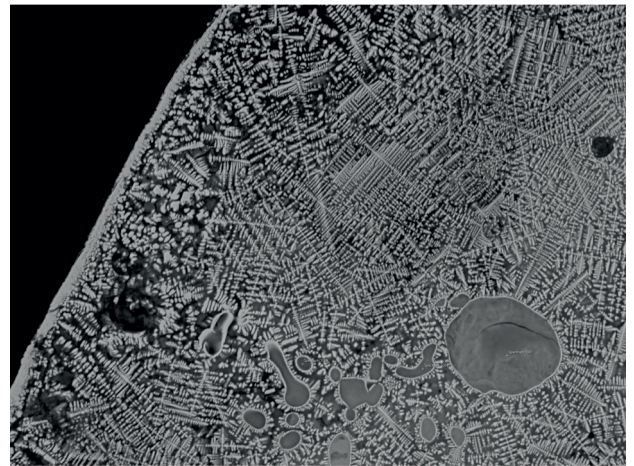
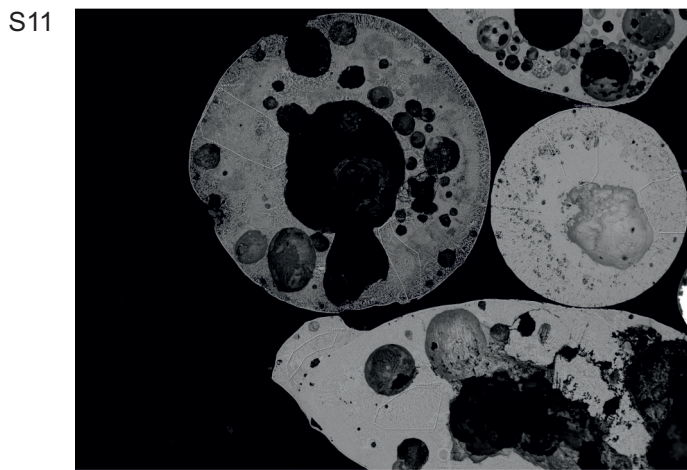
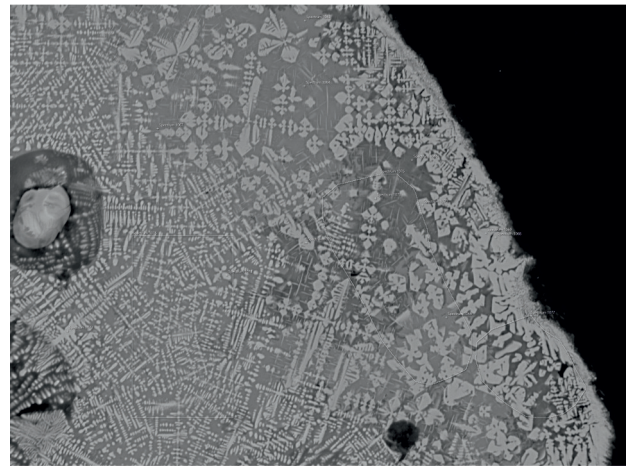
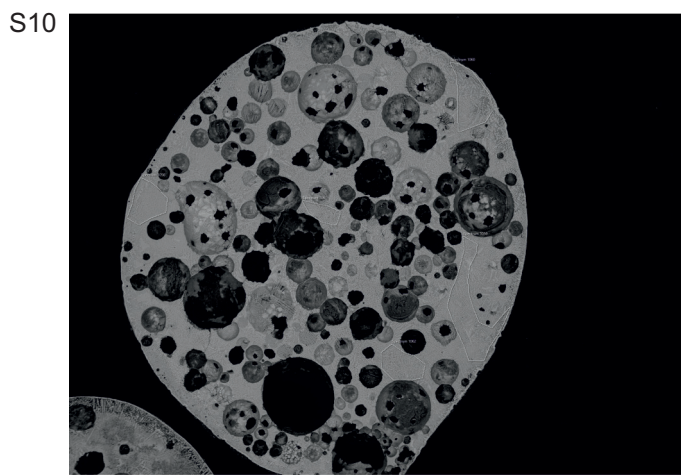
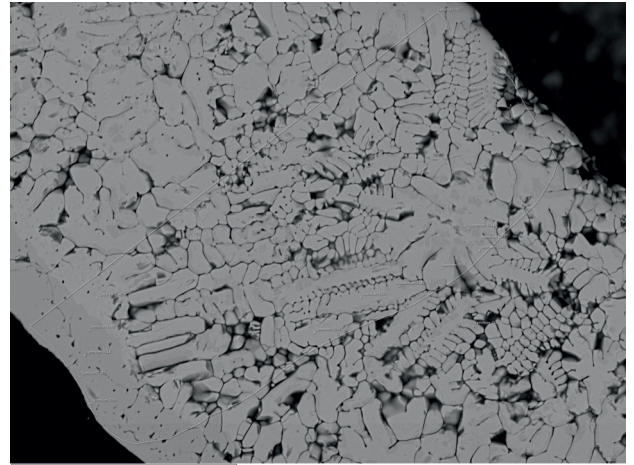
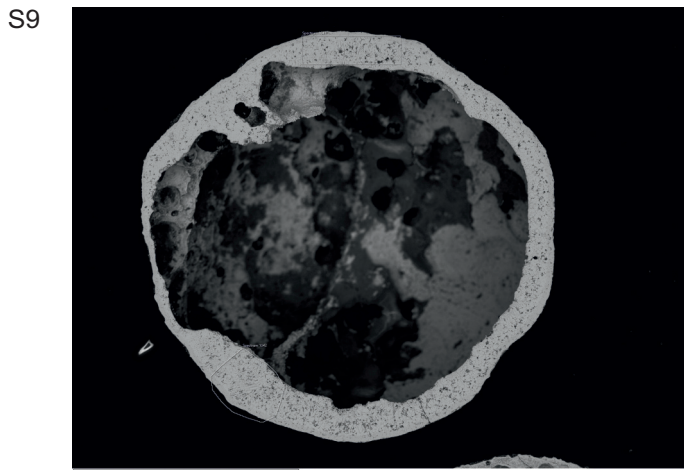


S7

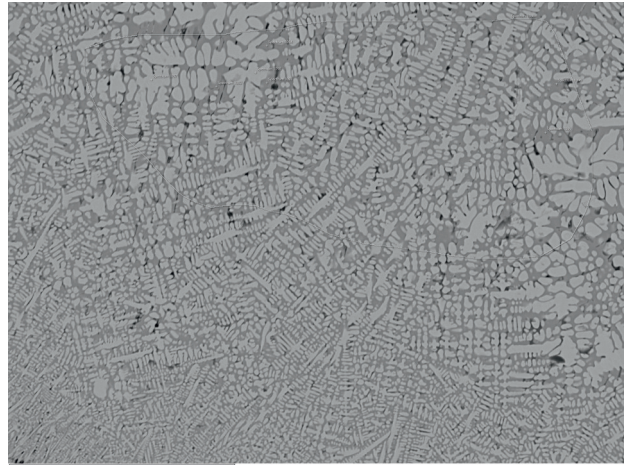


S8

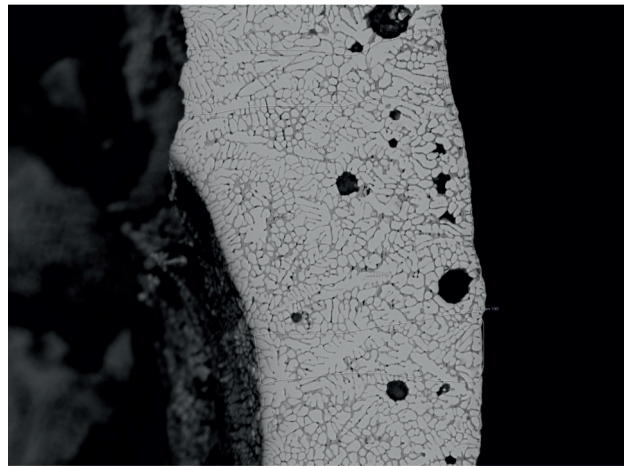
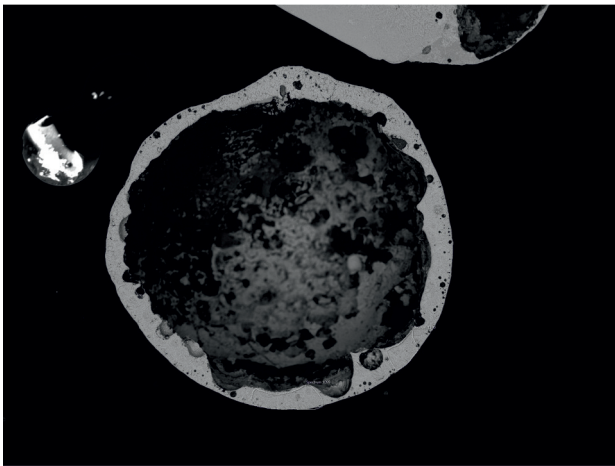




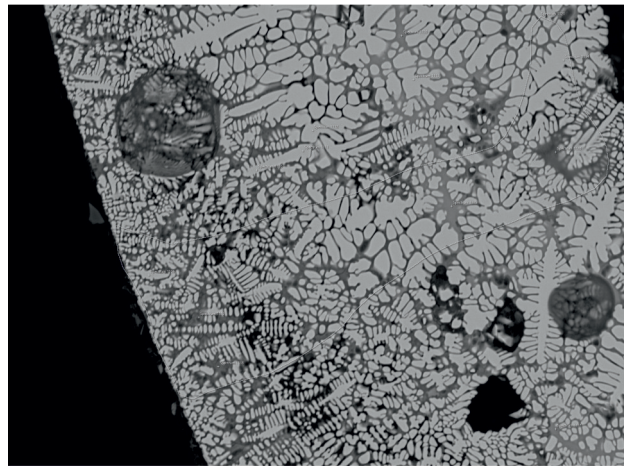
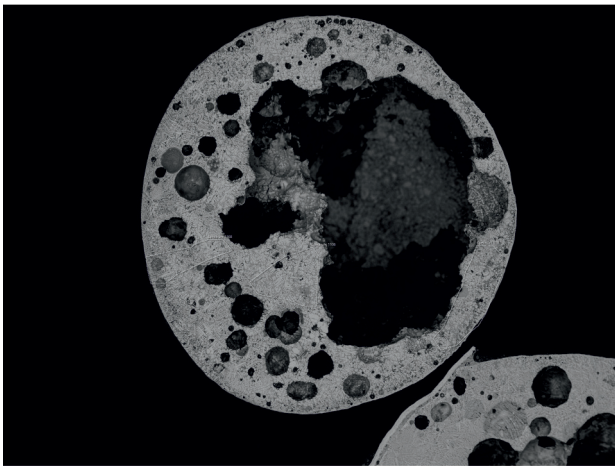
S13



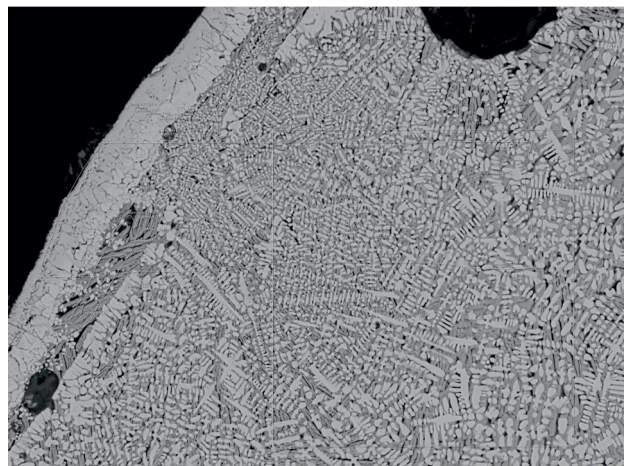
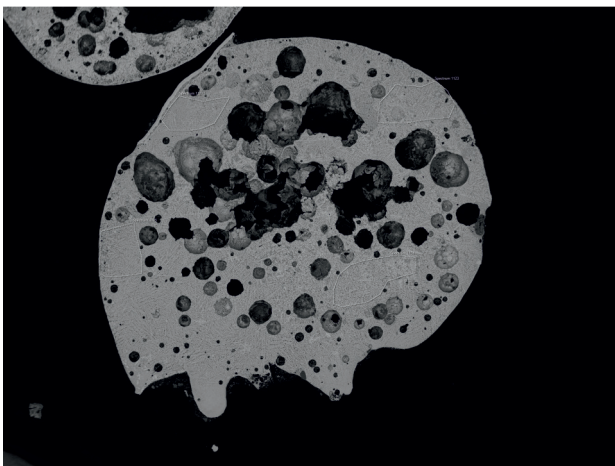
S14



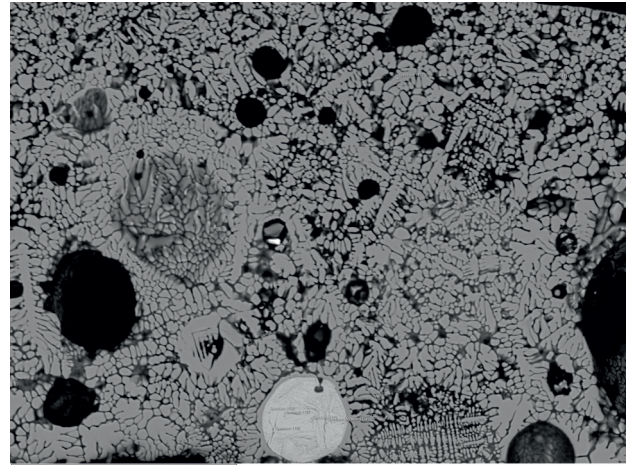
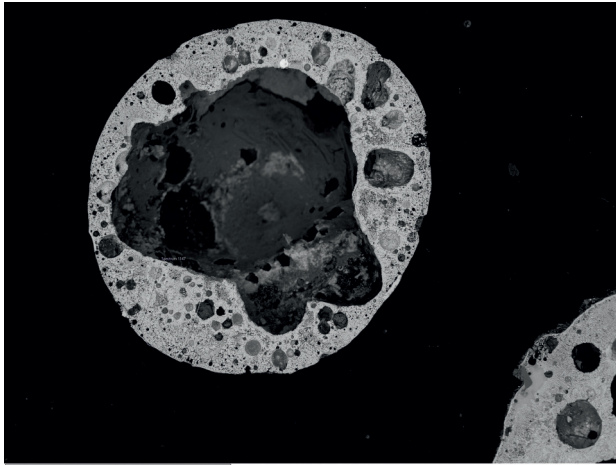
S15



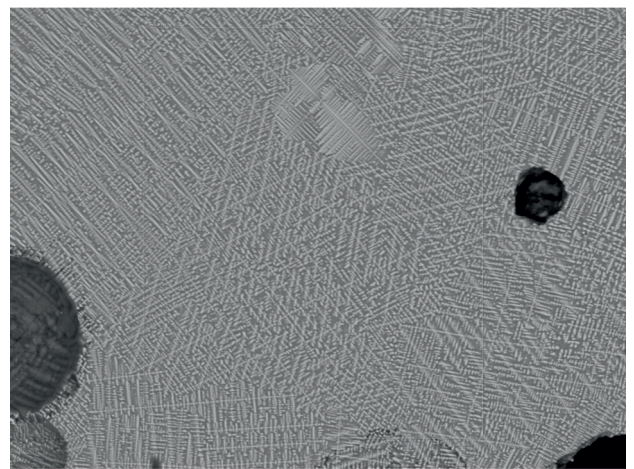
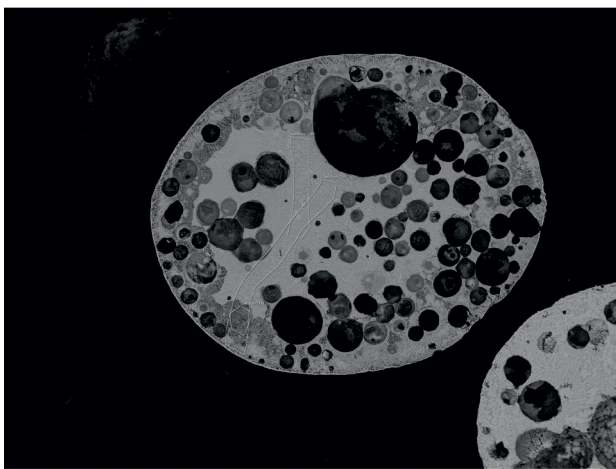
S16



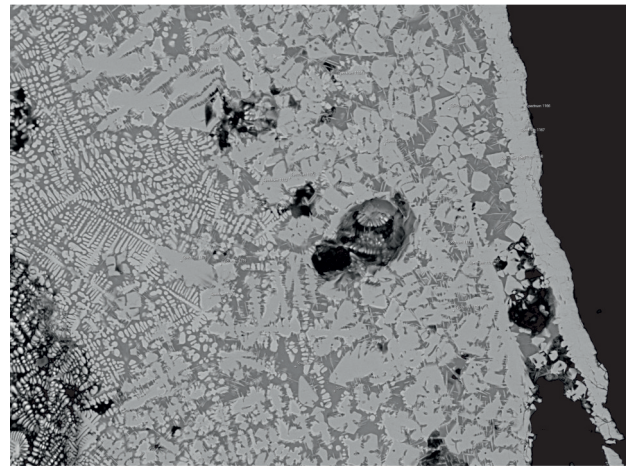
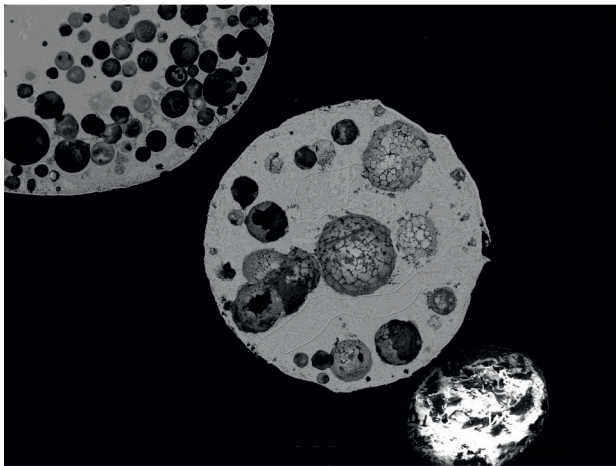
S17



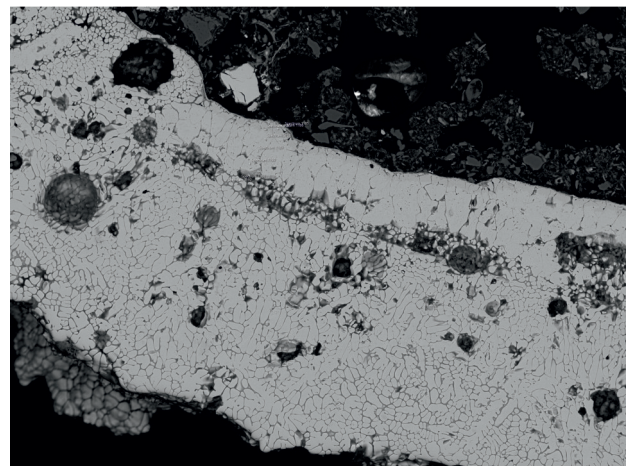
S18



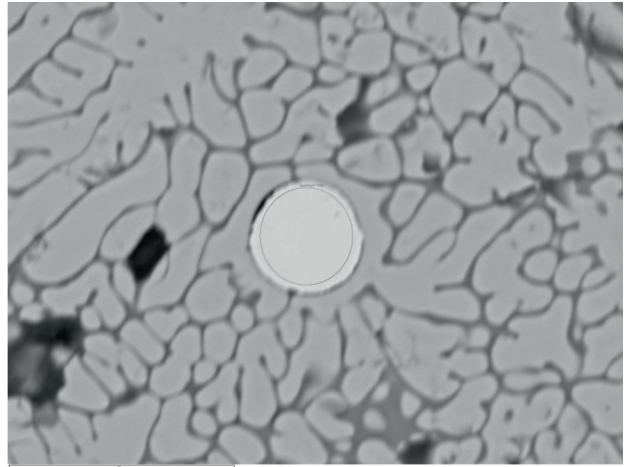
S19



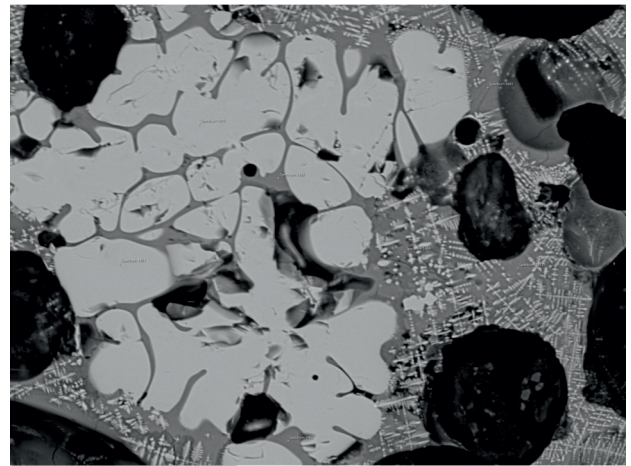
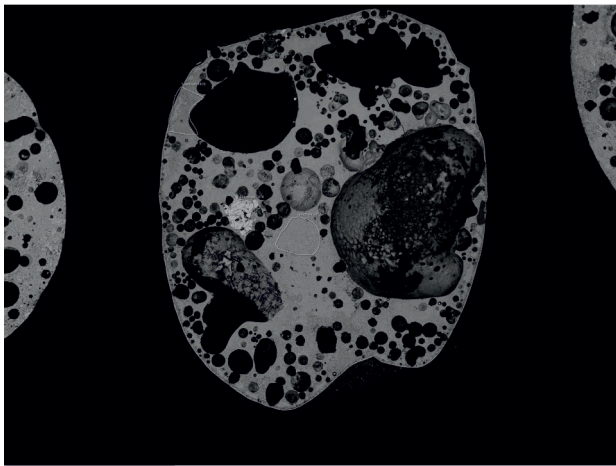
S20



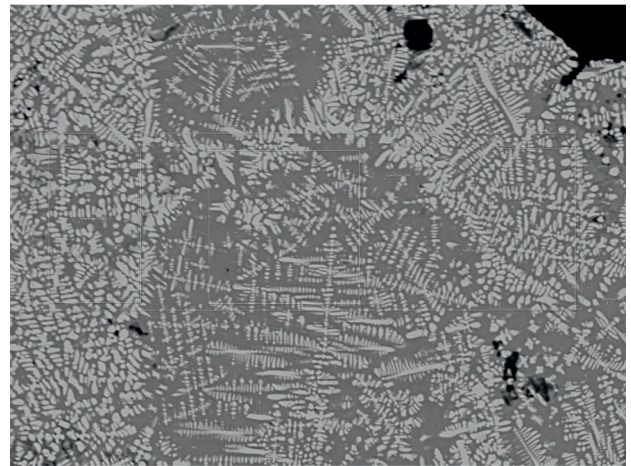
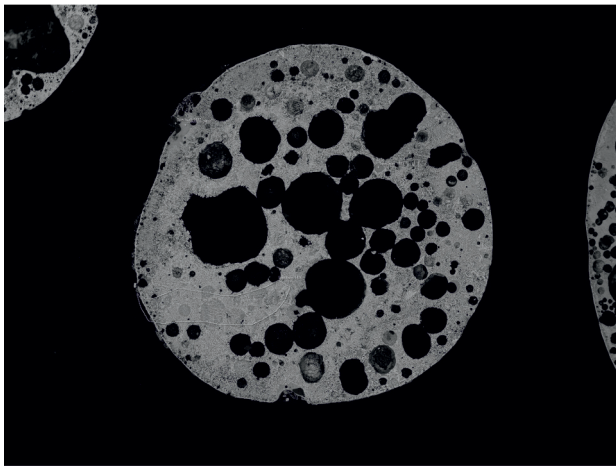
S20



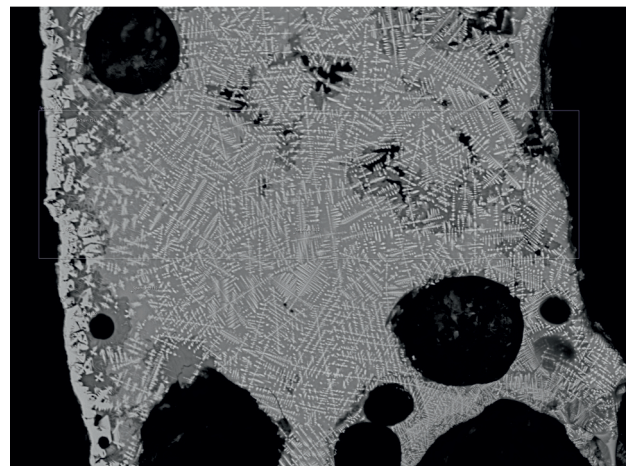
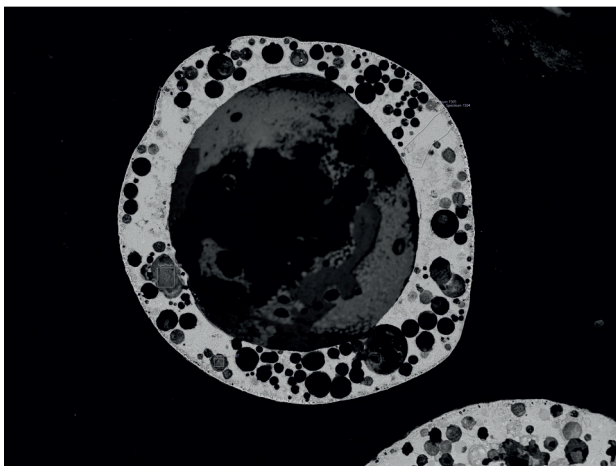
S21



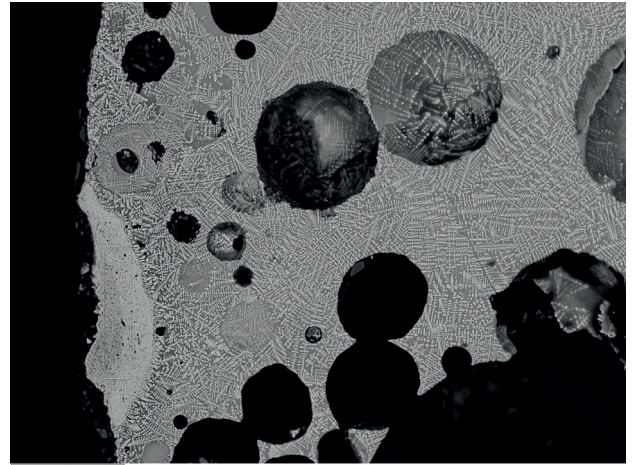
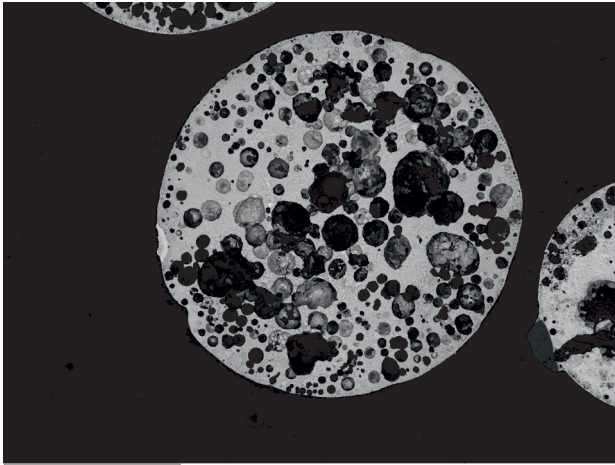
S22



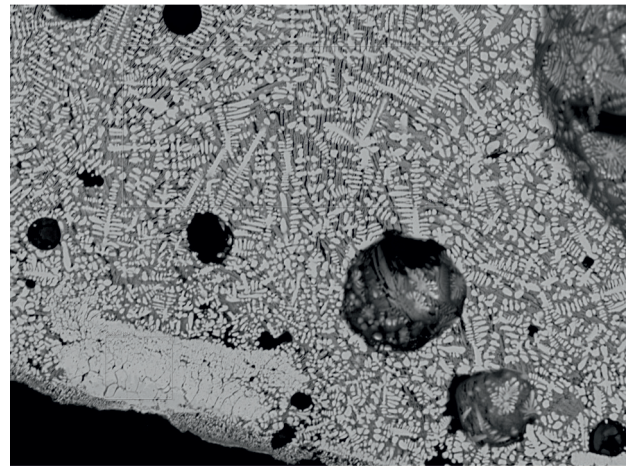
S23



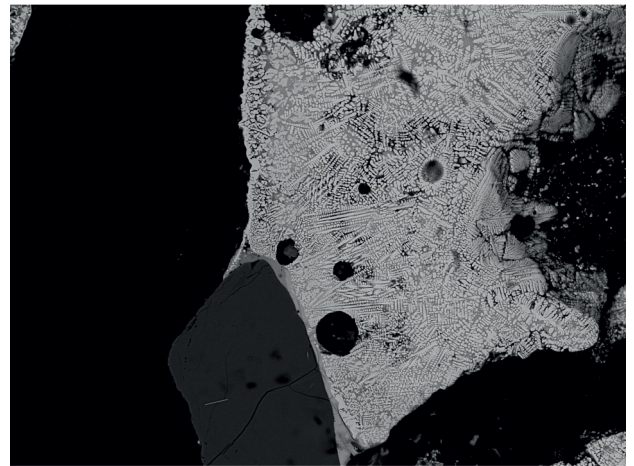
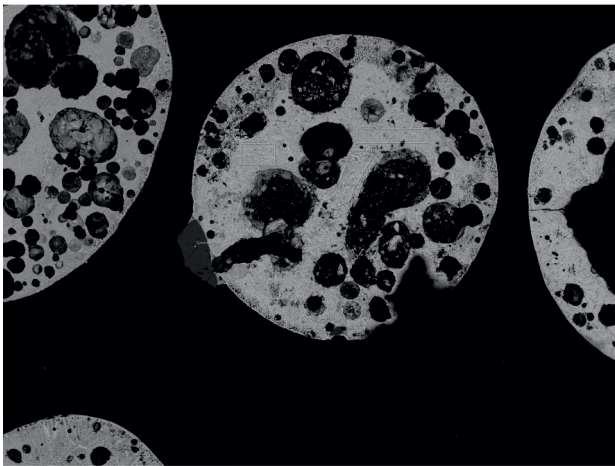
S24



S25



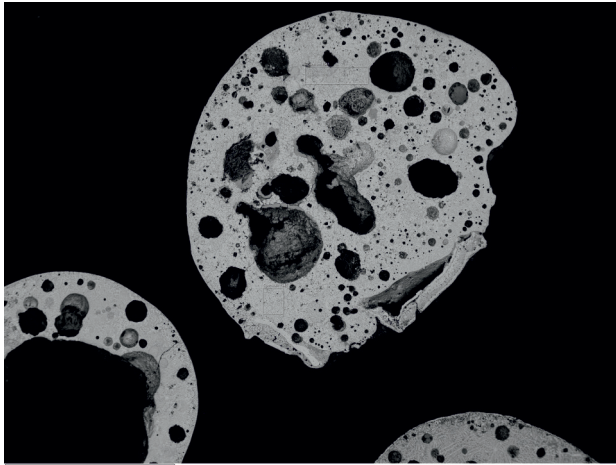
S26



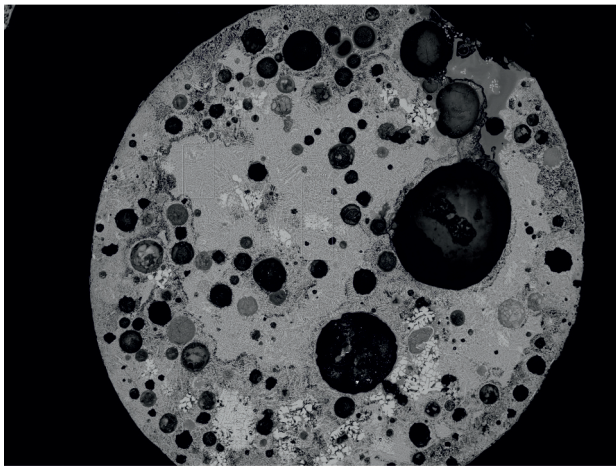
S27



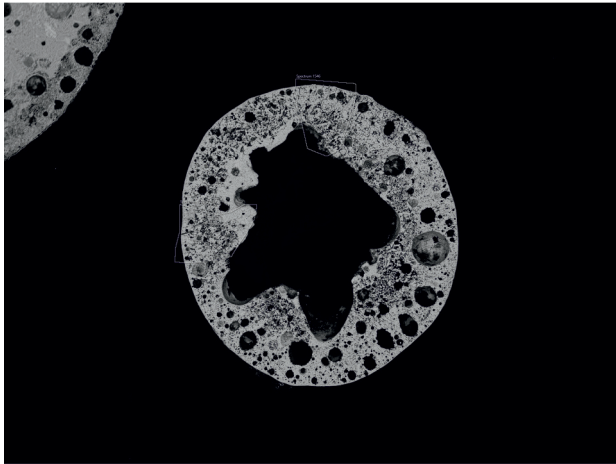
S28



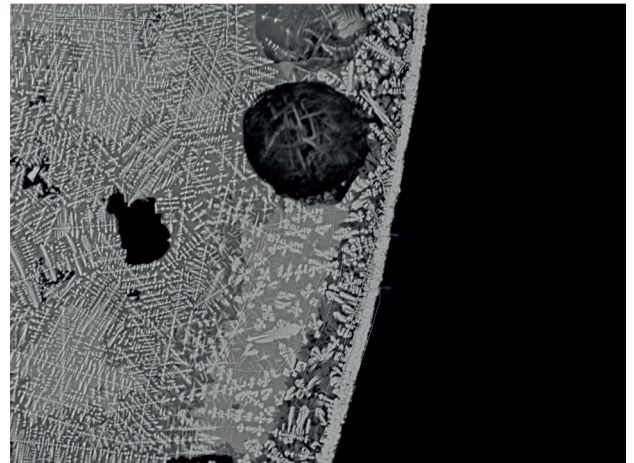
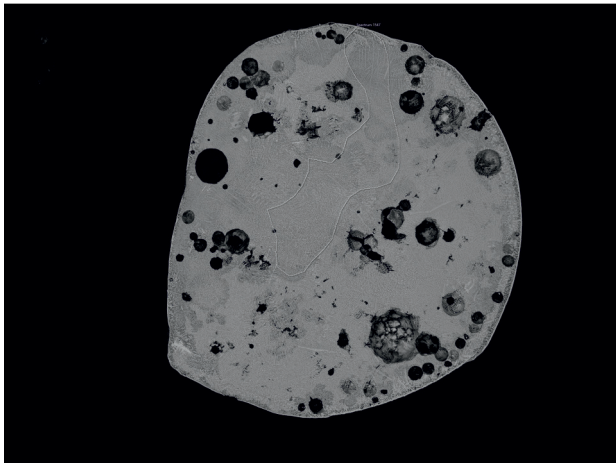
S29



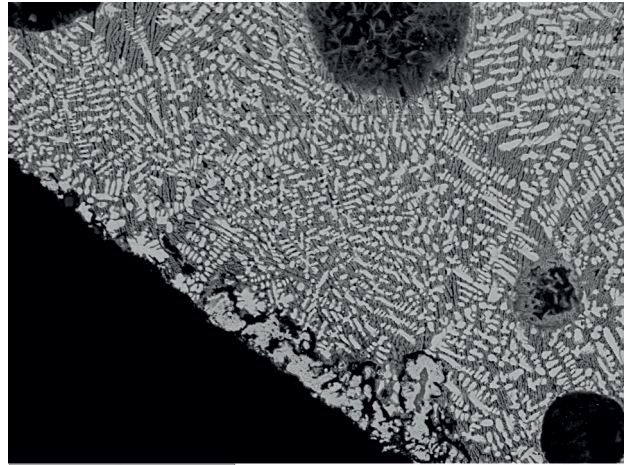
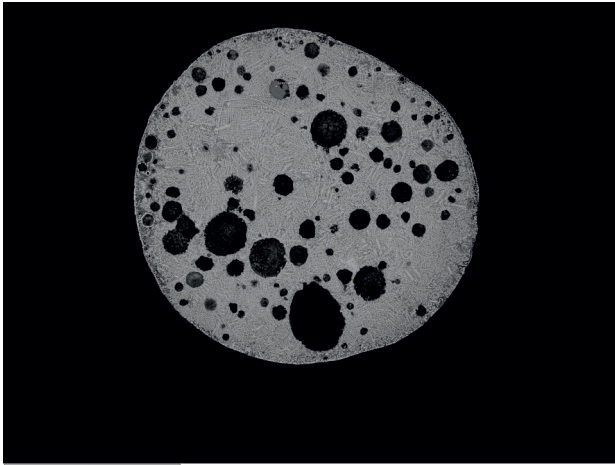
S30



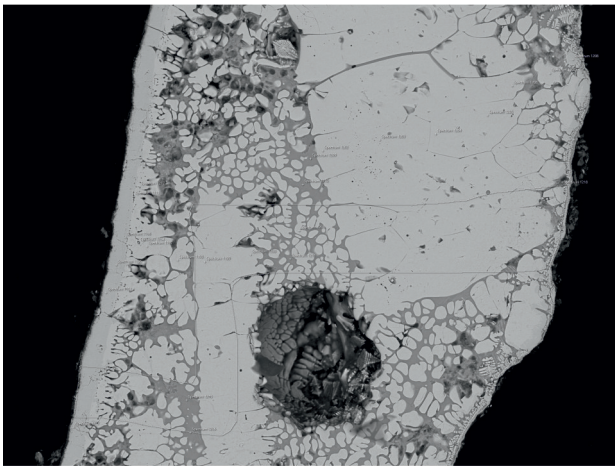
S31



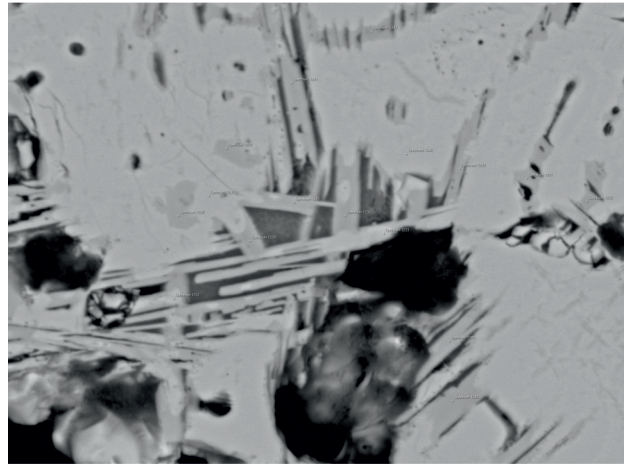
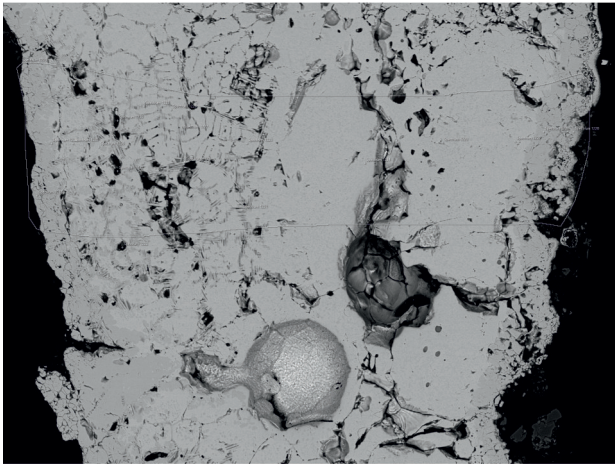
S32



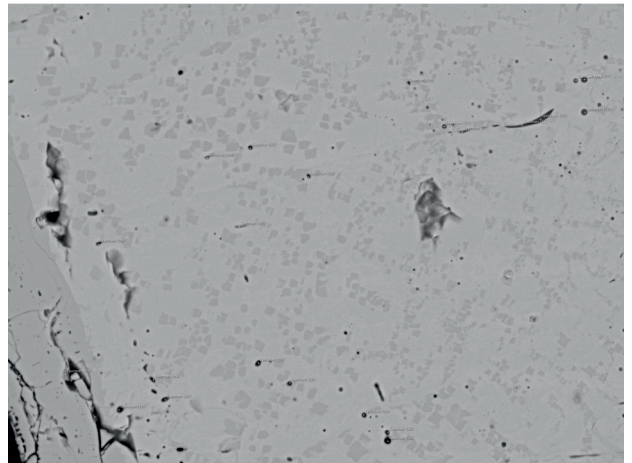
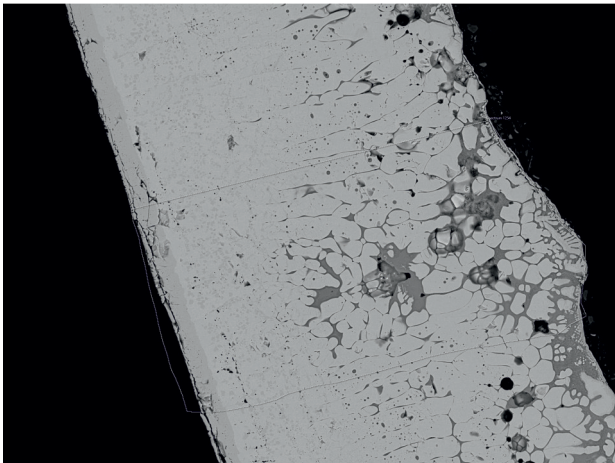
T1

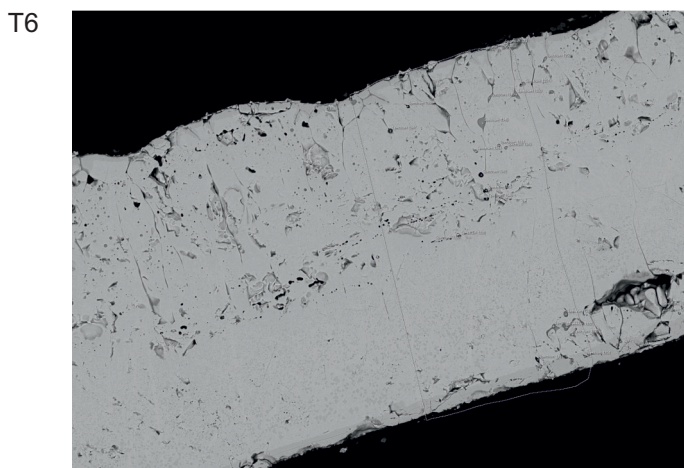
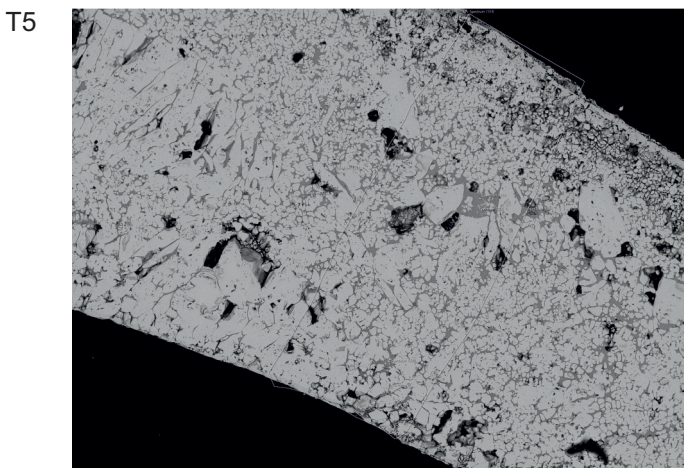
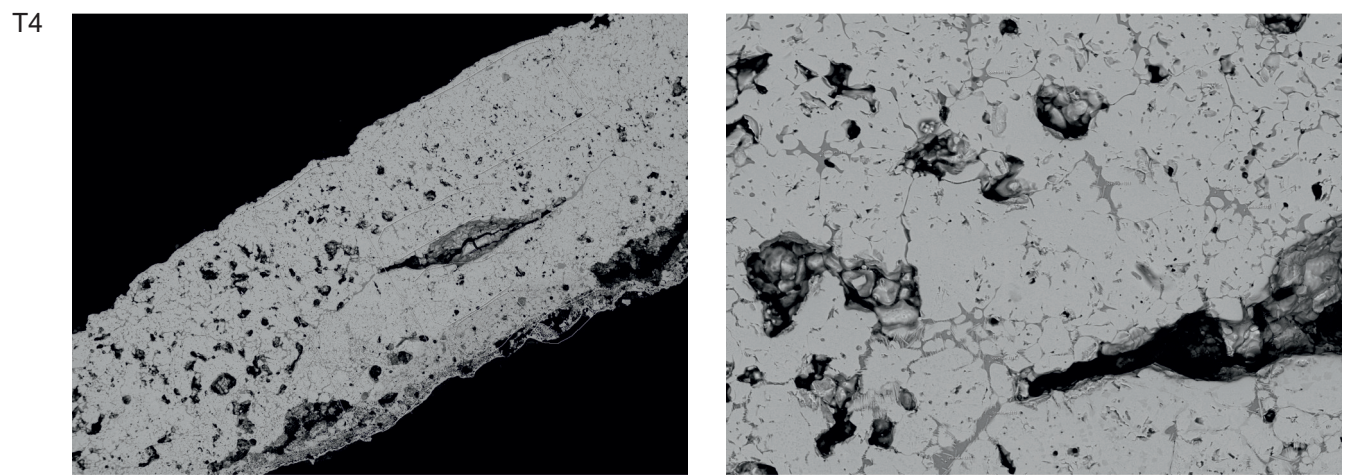
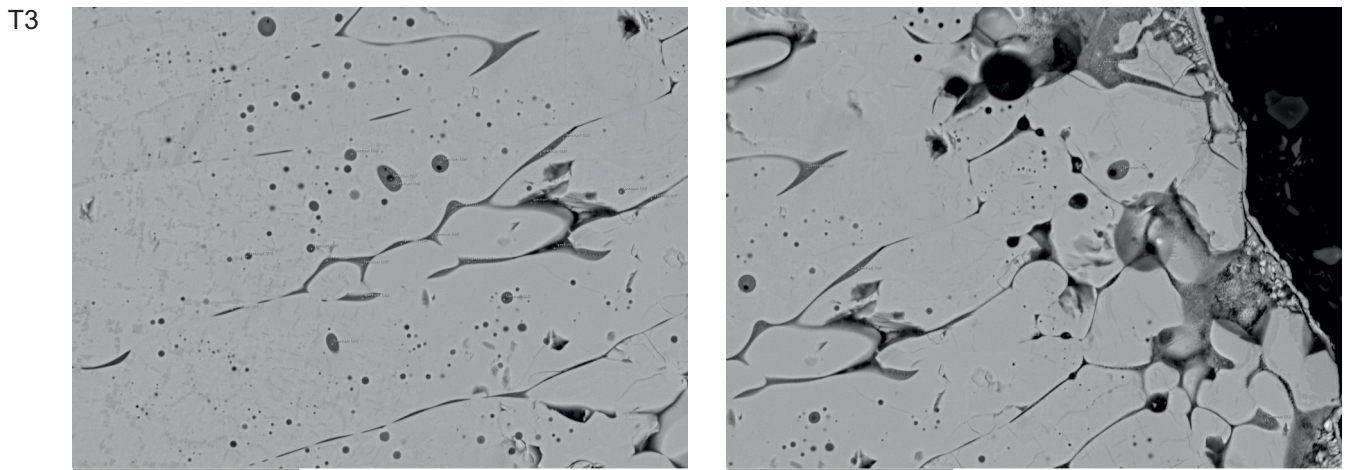


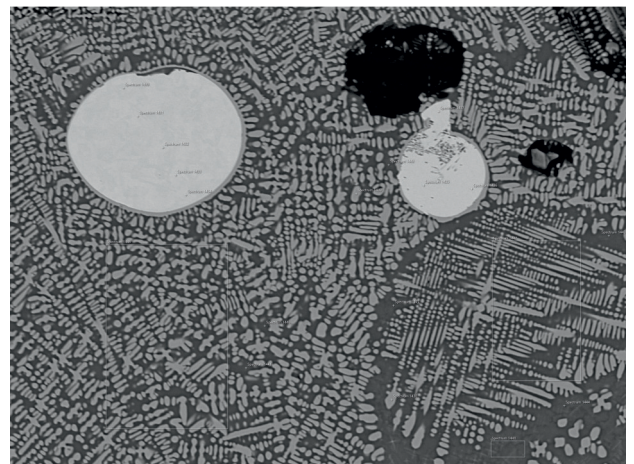
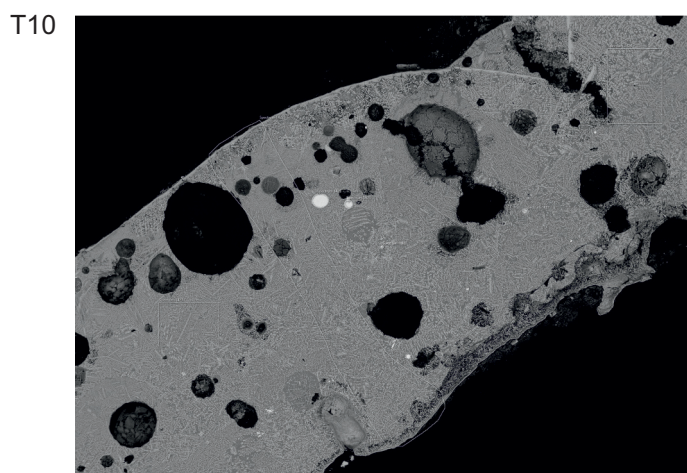
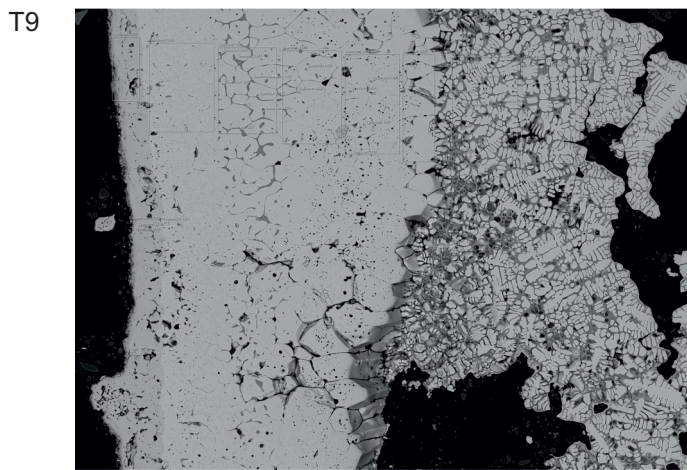
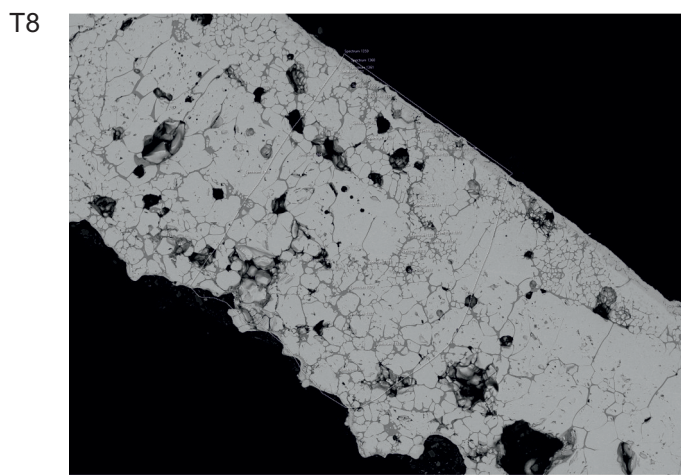
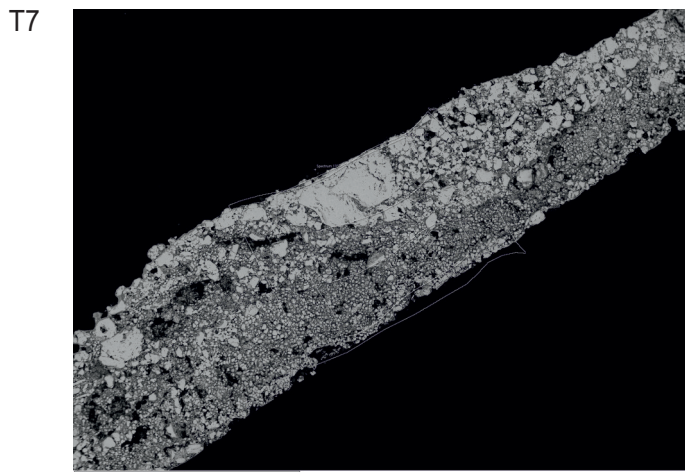
T2



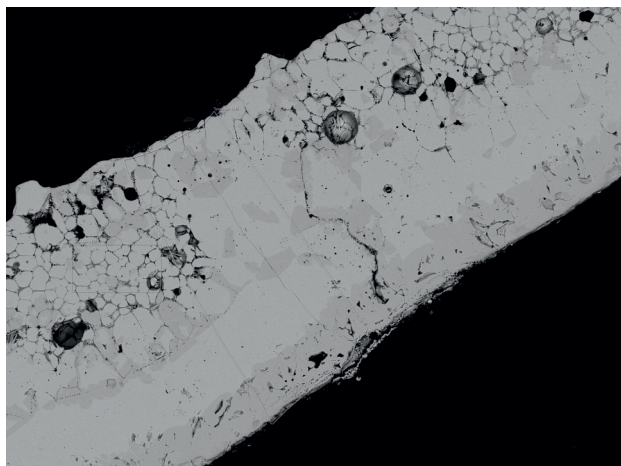
T3



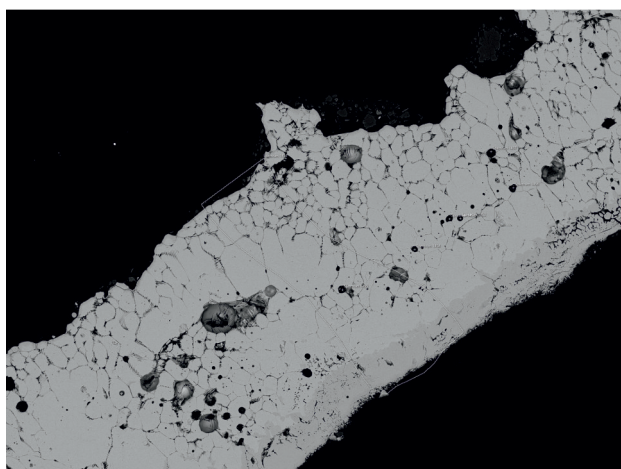




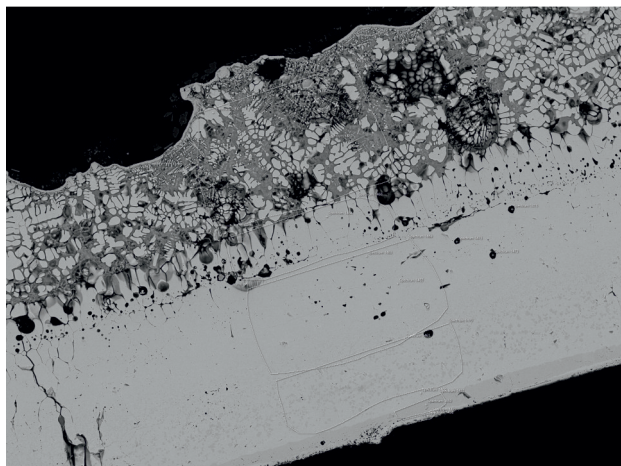
T1



T12



T13



GeoArch



geoarchaeological, archaeometallurgical & geophysical investigations

Unit 6,
Western Industrial Estate,
Caerphilly,
CF83 1BQ

Office: 029 20881431
Mobile: 07802 413704

E-Mail: Tim.Young@GeoArch.co.uk
Web: www.GeoArch.co.uk